Journal of Hydrology 573 (2019) 220–234

Contents lists available at ScienceDirect

Journal of Hydrology

journal homepage: www.elsevier.com/locate/jhydrol

Research papers

Significant differences exist in lake-atmosphere interactions and the evaporation rates of high-elevation small and large lakes

Binbin Wang[a,b,c,*,1], Yaoming Ma[a,b,d,*,1], Yan Wang[e], Zhongbo Su[c,1], Weiqiang Ma[a,b]

[a] Key Laboratory of Tibetan Environment Changes and Land Surface Processes, Institute of Tibetan Plateau Research, Chinese Academy of Sciences, Beijing 100101, China
[b] CAS Center for Excellence in Tibetan Plateau Earth Sciences, Chinese Academy of Sciences, Beijing 100101, China
[c] Faculty of Geo-Information Science and Earth Observation, University of Twente, Enschede 7500AE, the Netherlands
[d] University of Chinese Academy of Sciences, 100049 Beijing, China
[e] Department of Earth System Science, Tsinghua University, Beijing 100084, China

ARTICLE INFO

This manuscript was handled by Marco borga, Editor-in-Chief, with the assistance of Marco Toffolon, Associate Editor

Keywords:
Lake water and heat budget
Lake boundary layer parameters
Evaporation
Nam-Co basin
Tibetan Plateau

ABSTRACT

Lakes impact atmosphere boundary layer processes and are thus important for catchment scale climate modeling and regional water and heat budgets. To explore the differences in lake-atmosphere interaction parameters, meteorological variables and turbulent heat fluxes in small and large water bodies, we collected eddy covariance observations and meteorological data during ice-free periods of the Lake small Nam-Co ("small lake") in 2012–2013 and Lake Nam-Co ("large lake") in 2015–2016 on the Tibetan Plateau. Significant differences exist in their lake-atmosphere interaction processes due to differences in their inherent attributes and environmental backgrounds. Relative to the "small lake", the maximum surface temperature of the "large lake" in summer is approximately 3 °C lower; "large lake" also has a larger wind speed, a higher monthly average air temperature and delayed peaks of the seasonal variation of water and air temperature. The typical values of the roughness length and standard bulk transfer coefficient for momentum are approximately 80% and 21% higher, respectively, for the "large lake". The typical values of the roughness lengths for heat and water are one order of magnitude lower in the "large lake" while the corresponding standard bulk transfer coefficients are only 7% lower. The latent and sensible heat fluxes of the two lakes have quite different seasonal variations, with evaporation peaking in November for the "large lake" and in June for the "small lake". The estimated evaporation during the ice-free season of the "large lake" (approximately 981 ± 18 mm) is also higher than that (812 mm) of the "small lake" and this is mainly related to the observed lower Bowen ratio in the "large lake".

1. Introduction

As an important component of the climate system, lakes relative to other underlying surfaces have the characteristics of transparency to visible solar radiation, low albedo, small momentum roughness length, high thermal conductivity and large thermal capacity. They can impact atmosphere boundary layer processes in numerical climate modeling and affect local atmosphere circulation and regional heat and water budgets (Gerken et al., 2014; Long et al., 2007). A much higher latent heat flux (*LE*) than sensible heat flux (*H*) exists over the lake surface (Wang et al., 2015; Wen et al., 2016), thus yielding a lower lifting condensation level and higher boundary layer equivalent potential temperature, which favor convective precipitation (Small and Kurc, 2001). Because the heat capacity in lakes with different areas, depths, meteorological and environmental conditions differ between small and large water bodies, lakes may lead to quite different phase shifts of seasonal changes in meteorological variables and turbulent heat fluxes; thus lakes can impact the regional climate differently.

Lakes affect the overlying atmosphere through the lake-air turbulent heat flux, which is not only related to lake surface conditions (surface temperature, waves, water plants, etc.), but is also influenced by meteorological and environmental characteristics (warm-dry/cold-moist air, cloud cover, lake area, lake depth, etc.) (Blanken et al., 2003; Li et al., 2015a; Rouse et al., 2005; Wang et al., 2015; Wen et al., 2016). Gao et al. (2009) found that momentum roughness lengths differ between coastal shallow water and open sea, and these coefficients should be parameterized differently. Wang et al. (2015) have also found that the Charnock number (see definition in Charnock, 1955) for deriving the momentum roughness length is much higher in a small lake than the widely used values in oceanic research. Panin et al. (2006) suggest that

* Corresponding authors at: Building 3, Courtyard 16, Liucui Road, Chaoyang District, Beijing City 100101, China.
E-mail addresses: wangbinbin@itpcas.ac.cn (B. Wang), ymma@itpcas.ac.cn (Y. Ma), z.su@utwente.nl (Z. Su).
[1] They contribute equally to the manuscript.

https://doi.org/10.1016/j.jhydrol.2019.03.066
Received 18 September 2018; Received in revised form 14 March 2019; Accepted 18 March 2019
Available online 25 March 2019

Table 1
Summary of relevant lake studies on the Tibetan Plateau (the current paper is added for completeness). In the "Key results" column the components mentioned above are identified by the code: (1)quantify lake evaporation and its trend; and (2) issues related to energy budget or water balance. Studies that do not assess the two components have N/A directly following the code.

Study	Method used	Lake	Key results
Wang et al. (2017)	EC and Bulk method	Lake small Nam-Co	(1) Average value of 812 mm during open water periods in 2012 and 2013 (2) Estimated energy budget closure value of 0.97
Lazhu et al. (2016)	Flake model	Lake Nam-Co	(1) Average annual value of 832 ± 69mm during 1980–2014, and an not significant increasing trend was reported (2) The change of evaporation has suppressed the recent expansion of Lake Nam-Co
Ma et al. (2016)	CRLE	Lake Nam-Co	(1) Averaged annual value of 635 mm during 1979–2012; and a slight decreasing trend was reported (2) The decreasing trend of evaporation is responsible for approximately 4% of the recent rapid expansion of Lake Nam-Co
Zhou et al. (2013)	Pan observation	Lake Nam-Co	(1) Approximately 600 mm during May to October in 2007–2011 (2) Subsurface water seepage exists in this area
Zhu et al. (2010)	Penman-Monteith model	Lake Nam-Co	(1) Average annual value of 1430 mm during 1971–2004 (2) The supply of water could not complement the need for evaporation and the increase in water volume
Zhang et al. (2011)	Penman-Monteith model	Lake Nam-Co	(1) Average annual value of 1184 mm during 1976–2009, and a decreasing trend was reported (2) N/A
Haginoya et al. (2009)	Bulk method	Lake Nam-Co	(1) Averaged annual value of 658 mm during 2006–2008 (2) N/A
Li et al. (2016)	EC observation	Lake Qinghai	(1) Average annual value of 826 mm during May 2013 to May 2015 (2) N/A
Li et al. (2007)	Pan observation	Lake Qinghai	(1) Average annual value of 924 mm during 1959–2000; (2) Water balance was primarily influenced by surface runoff and precipitation and less by evaporation and anthropogenic factors;
Shi et al. (2010)	Pan observation	Lake Qinghai	(1)Average annual value of 880 mm during 1958–2004, and a decreasing trend was reported (2) N/A
Guo et al. (2016)	EC observation	Lake Serling Co	(1) 417 mm during April 26 to September 26 in 2014 (2) N/A
Li et al. (2015a)	EC	Lake Ngoring	(1) Average value of 436 mm during June to November in 2011–2012 (2) N/A
Liu et al. (2014)	EC	Lake Erhai	(1) Annual evaporation of 1165 mm in 2012 (2) N/A
Yu et al. (2011)	Bulk method	Lake Yamdrok Yum Co	(1) Average annual value of 1252 mm during 1961–2005, and a decreasing trend of $-2.4\ mm\ year^{-1}$ was reported (2) N/A
Xu et al. (2009)	Bulk method	Lake Yamdrok Yum Co	(1) Average annual value of 621 mm during 1961–2005, and a decreasing trend of 7% during warm season (May to September) in 1961–2005 was reported (2) N/A
Liu et al. (2009)	Pan observation	Lake Zigetang and Cuona	(1) Mean evaporation value of approximately 950 mm, and a decrease of annual evaporation since 1990 s (2) Lake growth was related to increase in annual precipitation and runoff and a decrease in evaporation
Li et al. (2001)	Penman method	Lake Zigetang	(1) Average annual value of 925 mm during 1958–1998, and an increasing trend was reported (2) N/A
Morrill (2004)	Lake energy balance model	Lake Ahung Co	(1) Annual value of approximately 760 mm during 1986–2001 (2) Precipitation plays significant role in the overall water balance, while the influence from evaporation is small
This study	EC and Bulk method	Lake Nam-Co and Lake small Nam-Co	(1) Annual evaporation value of approximately 981 ± 18 mm during the open water period of 2016. Significant differences exist in evaporations of Lake Nam-Co and the adjacent small lake (2) Energy budget closure value is 0.859 during the observational periods of July to November

shallower lake depths could result in higher bulk transfer coefficients and a larger lake-air turbulent heat flux. However, Venalainen et al. (1999) found a larger evaporation rate for a larger water body due to its higher wind speed. Except for the above issues, the thermal effect of sediments on water temperature in small and shallow lakes is appreciable, while such effect could be neglected in large and deep lakes (Fang and Stefan, 1996). Thus, what are the differences in lake-atmosphere transfer parameters, meteorological variables and turbulent heat flux between small and large water bodies, especially those locate close together and lying in same climatic background? Such related studies and publications are quite limited worldwide, and none exist on the high-elevation lakes of the Tibetan Plateau (TP).

Lake evaporation is an important component in the catchment scale hydrological cycle, energy budget and water balance analysis (See Table 1 for collected references on topics of lake evaporation and evaporation-related issues in the TP). All kinds of methods have been used for the estimation of evaporation in these high-elevation lakes on the TP. However, the reported evaporation from Pan observations and all kinds of model simulations for the same lake (i.e., Lake Nam-Co) show very large discrepancy in their seasonal variations and annual amounts (Lazhu et al., 2016; Ma et al., 2016; Wang et al., 2017; Wu et al., 2014; Xu et al., 2009; Zhu et al., 2010). The difference in estimated evaporation, i.e., approximately 600 mm in Zhou et al. (2013) and approximately 1430 mm in Zhu et al. (2010) in Lake Nam-Co, could lead to contrary water balance conclusions. Moreover, models such as the fresh-water lake model (Flake) (Lazhu et al., 2016) and the complementary relationship lake evaporation (CRLE) model (Ma et al., 2016) have recently been used to derive evaporation in Lake Nam-Co; however, opposite evaporation trends have been reported using the same forcing data. These inconsistencies may result from the fact that: (1) Pan evaporation, widely used as a validation dataset for actual lake evaporation, may result in significant errors due to the differences in sizes of water bodies and the differences in their overlying atmosphere and environments; and (2) the model simulations by the bulk transfer method, the Flake model, the CRLE model and the Penman-Moteith method are widely used in lake-atmosphere heat flux simulation (Wang

et al., 2015; Wang et al., 2017; Xu et al., 2009; Yu et al., 2011); however, these methods need validation and evaluation in advance rather than referring to existing published parameterization schemes performed for other low-elevation lakes (Xu et al., 2009; Yu et al., 2011). Thus, to clarify the above issues, lake-atmosphere turbulent heat flux observations by a direct eddy covariance (EC) system are needed.

Eddy covariance systems (listed in Nordbo et al., 2011) have been applied to all kinds of lakes around the world (Granger and Hedstrom, 2011; Liu et al., 2012; Mammarella et al., 2015; Tanny et al., 2008; Zhang and Liu, 2014), and recently on several high-elevation lakes of the TP (Biermann et al., 2013; Li et al., 2016; Li et al., 2015b; Liu et al., 2014; Wang et al., 2015, 2017; Wen et al., 2016). However, none of the above studies focused on the differences that exist between small and large lakes due to the difficulty in measurements of high-elevation lakes on the TP. In this study, using EC observations in the two adjacent lakes of Lake small Nam-Co (Wang et al., 2015, 2017) and Lake Nam-Co, we aim to achieve two specific objectives: (i) to illustrate clearly the differences that exist in the boundary layer parameters, meteorological conditions and turbulent heat fluxes of the two water bodies; and (ii) to quantitatively obtain the evaporation and energy budget of Lake Nam-Co during its ice-free season. The objectives could address the following general questions: (1) what differences exist between small and large water bodies in lake-atmosphere boundary layer processes; and (2) whether evaporation estimated in smaller water bodies is appropriate for the evaluation of evaporation in larger water bodies. The deployment of instruments and data are introduced in Section 2. Data processing and methods are explained in Section 3. The results are reported in Section 4. Specifically, in Section 4.1, we compared the boundary layer parameters of the two lakes and evaluated several lake-air boundary layer parameterization schemes. In Section 4.2, the turbulent heat flux simulated by the bulk transfer method with optimized parameterization schemes, is evaluated by high-quality EC observations. In Section 4.3, the differences in meteorological variables and the turbulent heat fluxes of the two lakes are depicted. In Section 4.4, the evaporation and energy budget analysis of the Lake Nam-Co are described. Lastly, Discussions and Conclusions are provided in Sections 5 and 6, respectively.

2. Study site and materials

Being considered as Asia's water tower and consisting of more than 1200 lakes larger than 1 km^2 in surface area and tens of thousands of small lakes (Zhang et al., 2014), the TP, with an average elevation of approximately 4000 m above sea level, forms the largest high-elevation inland lake zone in the world (Ma et al., 2011; Zhang et al., 2014). The water resources, hydrological cycle and ecological change in the TP have attracted significant attention for scientific research based on the limited field measurements (Immerzeel et al., 2010; Oku et al., 2006; Singh and Nakamura, 2009; Wei et al., 2012; Yang et al., 2014). The Nam-Co Lake Basin, with an area of 10610 km^2, lies in a transition region of semiarid and semihumid climatic zones in the central TP, and its climate could be influenced both by the westerlies and the South Asia summer monsoon. The target lakes contain adjacent two lakes: Lake Nam-Co (90°15′ − 91°03′E, 30°29′ − 30°56′N, "large lake" for short henceforth, Fig. 1a) and Lake small Nam-Co (90°58′10″E, 30°46′55″N, "small lake" for short henceforth, white box '1' in Fig. 1a and 1b1). The "large lake" is the third largest lake on the TP, with a surface elevation of approximately 4715 m a.s.l., an area of more than 2000 km^2 and a maximum depth of more than 90 m (Wang et al., 2009). The "small lake", with an area of 1.4 km^2 and a maximum depth of approximately 14 m, is located to the southeast of the "large lake". The distance between the two lakes is only approximately 500 m. According to field experiences, the start dates of ice-formation in the "small lake" and the "large lake" are around mid-November and the beginning of January, respectively, while the dates of ice-melt are near the beginning of April and beginning of May, respectively. In 2005, the first meteorological & hydrological station, the Nam-Co Monitoring and Research Station for the Alpine Environment (Nam-Co station, black circle in Fig. 1b1), was established, and it has provided enormous data for research in this catchment.

2.1. Measurements and instruments

The instruments in the "small lake" (Fig. 1b2), including an EC system, four component radiation sensors, a water level gauge and water temperature gradient probes, were installed 8 m off the shore in April 2012 and maintained until October 2014. Details about the site description, instrument settings, data processing and results for the "small lake" can be found in (Wang et al., 2015, 2017). The observation site in the "large lake" is situated on an island (an area of approximately 0.18 km^2, white box '2' in Fig. 1a and 1c1). The instruments are setup at the southwest of the island and include the following observations: (1) on July 28th, 2015, an automatic weather station (AWS, Fig. 1c2) was established on the island and is approximately 10 m far from the shore. The meteorological variables consist of two levels of air temperature, air humidity, wind speed and wind direction at heights of 1.52 m and 9.52 m above the land surface. In addition, air pressure, precipitation and four component radiation are also observed. The AWS system is sampled by a CR1000 data-logger every 10 min, and it is powered by a 12-volt battery and charged by solar panels. (2) On July 7th, 2016, an EC observation system (insert in upper left of Fig. 1c2, facing south) is added in the AWS tower at a height of 4.5 m above the island surface (another 1.5 m above the water surface). Temperature, humidity and three-dimension wind speeds are measured at a frequency of 10 Hz by a gas analyser (Li-7500A, LI-COR Biosciences) and ultrasonic anemometer (CSAT3, Campbell Scientific, Inc.), respectively, and the data are collected by a second CR1000. (3) A water temperature profile to a depth of 35 m (90.7979 E, 30.8107 N) is installed from July 28th to November 19th in 2015 and from July 7th to November 18th in 2016, respectively. The temperature sensors are distributed at 10 depths (0.5 m, 1.5 m, 3 m, 6 m, 10 m, 15 m, 20 m, 25 m, 30 m, 35 m) and are affixed to a floating buoy weighted to the lake bottom. The sensor at a depth of 30 m was damaged in 2016. The temperature at the 0.5 m depth is chosen as the water surface temperature (T_s, °C) (more details see Section 3.1). The specifications of the stations in the "small lake" and the "large lake" are summarized in Table 2. In addition, the Nam-Co station (black circle in Fig. 1b1), including a planetary boundary layer tower (wind speed, wind direction, air temperature and air humidity, air pressure at 5 layers) and four component radiation sensor over the grassland, provides supplemental data of the Nam-Co Basin (Ma et al., 2014). Furthermore, MODIS LST products (MOD11A1 and MYD11A1) at a spatial resolution of 1 km in 2016 are also used.

3. Methodology

3.1. Processing of eddy covariance data

Half-hourly H and LE in the "small lake" and the "large lake" could be accessed by processing the high frequency EC observations using the "Turbulence Knight 3" software (https://zenodo.org/record/20349#). All the relevant corrections (time lag compensation, spike removal, planar fit rotation, spectral correction, and Webb-Pearman-Leuning density correction) are included (Mauder and Thomas, 2015). To compare the lake-atmosphere interaction parameters (roughness lengths and bulk transfer coefficients for momentum, heat and water), these coefficients could be calculated through the well-known boundary layer theory (see Supplementary material for more information). The meteorological variables and bulk transfer coefficients have a height dependency. For example, a logarithm relationship between wind speed and height exists. Thus, after deriving z_{0m}, z_{0h} and z_{0q} using observations, U_z (m s^{-1}), T_z (°C) and q_z (kg kg^{-1}) should be corrected to a reference height of 10 m and a neutral atmosphere. Furthermore, the

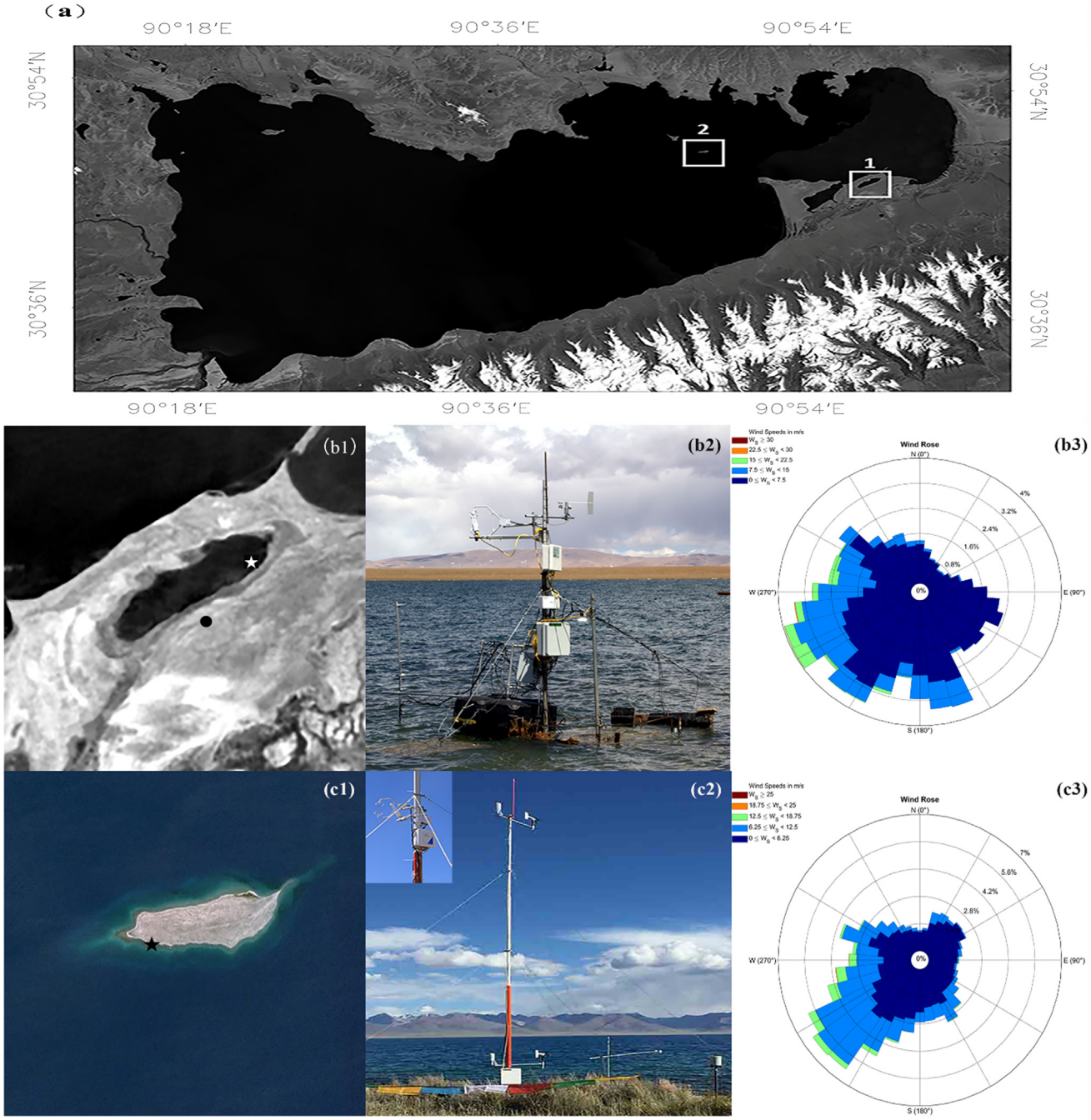

Fig. 1. (a) The positions of observation sites of the "small lake" (white box '1') and the "large lake" (white box '2') in the Nam-Co Basin; (b1) the enlarged view of the "small lake" area; the white pentagram shows the position of the measurements in the "small lake" while the black circle shows the position of "Nam-Co station"; (b2) the photo of the instruments; (b3) the wind rose in the "small lake" area; (c1) the enlarged view of the "large lake" area; the black pentagram indicates the position of the measurements on the island of the "large lake"; (c2) the photo of the instruments; (c3) the wind rose in the "large lake" area.

C_{Dz}, C_{Hz} and C_{Ez} obtained in the "small lake" and "large lake" should also be adjusted to neutral conditions and a reference height of 10 m (C_{DN10}, C_{HN10}, C_{EN10}) (Andreas and Murphy, 1986) using Eqs. (1–3):

$$C_{DN10} = \frac{k^2}{[kC_{Dz}^{-0.5} - \ln\left(\frac{z}{10}\right) + \Psi_m(\zeta)]^2} \quad (1)$$

$$C_{HN10} = \frac{kC_{DN10}^{0.5}}{kC_{Dz}^{0.5}C_{Hz}^{-1} - \ln\left(\frac{z}{10}\right) + \Psi_h(\zeta)} \quad (2)$$

$$C_{EN10} = \frac{kC_{DN10}^{0.5}}{kC_{Dz}^{0.5}C_{Ez}^{-1} - \ln\left(\frac{z}{10}\right) + \Psi_q(\zeta)} \quad (3)$$

To ensure the data quality of EC observations, the following criteria are also considered: (1) data quality flags (1–9, "1″ indicates highest quality, "9" indicates lowest quality) considering the "steady state test" and the "integral turbulence characteristics test" are used for high-quality heat flux selection. More accurately, the turbulent heat flux with quality flags larger than 3 are discarded. (2) Similar to the footprint analysis in the "small lake" (Wang et al., 2015), the turbulent heat flux of the "large lake" from wind directions (WD < 135° & WD > 270°, with north as 0° and the azimuth increasing clockwise) contaminated

Table 2
Specifications of the field observations in the "small lake" and the "large lake"

Instruments	The "small lake" (Fig. 1b)	The "large lake" (Fig. 1c)
Ultrasonic anemometer	CSAT3 (Campbell Scientific, Inc.); 2.7 m above the water surface and face west; April 2012–October 2014	CSAT3 (Campbell Scientific, Inc.), approximately 6 m above the water surface and face south; July 2016–July 2018
Open path CO_2/H_2O analyzer	Li-7500A (LI-COR Biosciences), 2.7 m above the water surface and 25 cm south of the CSAT3; April 2012–October 2014	Li-7500 (LI-COR Biosciences), 6 m above the water surface and 20 cm west of the CSAT3; July 2016–July 2018
Water temperature	CSI109 (Campbell Scientific, Inc.), at depths of 0.05 m, 0.1 m, 0.15 m, 0.3 m, 0.6 m; April 2012–November 2013	HOBO water temperature Pro v2 Data Logger 021001, at depths of 0.5 m, 1.5 m, 3 m, 6 m, 10 m, 15 m, 20 m, 25 m, 30 m, 35 m; August 2015 – November 2015 and July 2016 – November 2016
Net radiometer	CNR1 (Kipp & Zonen), 1.5 m above the water surface; April 2012–November 2013;	CNR1 (Kipp & Zonen), 1.5 m above the land surface; August 2015 – present
Water level	10 min intervals; April 2012–November 2013	Manual observation, daily interval
Air temperature and humidity	——	HMP 155A (Vaisala), 1.52 m and 9.52 m above the land surface; August 2015–present
Wind speed and direction	——	RM Young wind Monitor, 1.52 m and 9.52 m above the land surface; August 2015 – preent
Rain gauge	——	Tipping bucket; August 2015 – present

by land are discarded, and the remaining turbulent fluxes have upstream fetches of more than 30 km and water depths of more than 90 m. (3) The impact of internal boundary layers caused by discontinuities of surface properties are also checked. The following fetch-height relationship was used to roughly estimate the height of the new equilibrium layer (δ): $z \geq \delta = 0.3\sqrt{x}$, where x is the fetch (m) and z is the height (m) of sensor. Thus, the internal boundary layer height caused by land is only approximately 1 m, which is much lower than the height of sensors. (4) Due to the strong influence of local free convection on turbulence for small wind, the turbulent heat flux for small wind ranges ($U_z < 3$ m s^{-1}) are also ignored in the estimation of boundary layer parameters. This criteria through U_z will also guarantee a fully mixed surface layer and justify the substitution of T_s by water temperature at a depth of 0.5 m. (5) Because roughness lengths show high sensitivity to measurement errors at small H and LE, turbulent heat fluxes smaller than 10 W m^{-2} are ignored. Additionally, the following criteria are considered as abnormal ranges of roughness lengths: $\ln(z_{om}) < -15$ or $\ln(z_{om}) > -5$; $\ln(z_{oh}) < -15$ or $\ln(z_{oh}) > -3$; $\ln(z_{oq}) < -15$ or $\ln(z_{oq}) > -3$. After all these quality controls, the EC observations could represent the lake-atmosphere interaction of the "large lake", and the valid data percentages are 54.8% with only wind direction criteria, 82.3% with only quality criteria, 83.8% with wind speed criteria and 42.4% with all three criteria. Moreover, we emphasize that the EC observations after quality control are used in the analysis of boundary layer parameters in Section 4.1, and the contaminated EC values are substituted by simulations from the bulk transfer method in Section 4.2. The details of the bulk transfer method can be found in Wang et al., 2015.

3.2. Parameterization schemes of roughness lengths

Roughness lengths for momentum, heat and water are important parameters in water-atmosphere turbulent transfer processes, and having reliable parameterization schemes of roughness lengths is still an unsolved issue for lakes on the TP. During the past several decades, various forms of roughness length parameterization schemes for water surfaces have been developed (Fairall et al., 1996; Liu et al., 1979; Smith, 1988; Vickers and Mahrt, 2010), including the one related with atmospheric stability conditions (Zilitinkevich et al., 2008). Parameterization schemes of momentum roughness lengths usually consider two situations: wind stress-related rough flow (Charnock, 1955; Smith, 1988) and the viscosity-related smooth flow. Right now, the most commonly used form is $z_{0m} = \alpha\frac{u_*^2}{g} + Rr\frac{\nu}{u_*}$ where ν is the kinematic viscosity of air (m^2s^{-1}), with a value of approximately $1.5 \times 10^{-5} m^2s^{-1}$ for the atmosphere at the sea level and approximately $2.4 \times 10^{-5} m^2s^{-1}$ at the high-elevation Lake Nam-Co. The Charnock number (α) and roughness Reynolds number (R_r) are optimized considering the specific wave effect of the "small lake" (Wang et al., 2015). In this study, P1 ($\alpha = 0.013$; $R_r = 0.11$) are considered "oceanic parameters" while P2 ($\alpha = 0.031$; $R_r = 0.54$) are "optimized parameters". Since the sensitivity of lake-air turbulent heat fluxes to the choice of algorithms of roughness lengths has been widely recognized (Webster and Lukas, 1992), the different forms of roughness lengths in Table 3 (mainly from appendix of Zeng et al., 1998) will be evaluated by our observations. The forms with the best performances will be further used for turbulent heat flux simulation using the bulk transfer method.

Table 3
Studied parameterization schemes for z_{0m}, z_{0h} and z_{0q}.

Methods	z_{0m}	z_{0h}	z_{0q}	Refs.
UA	$z_{0m} = \alpha\frac{u_*^2}{g} + R_r\frac{\nu}{u_*}$	$ln\frac{z_{0m}}{z_{0h}} = 2.67Re_*^{0.25} - 2.57$	$z_{0q} = z_{0h}$	Brutsaert (1982), Zeng et al. (1998)
CCM3	——	$z_{0h} = 2.2 \times 10^{-9}, \zeta > 0 z_{0h} = 4.9 \times 10^{-5}, \zeta < 0$	$z_{0q} = 9.5 * 10^{-5}$	Large and Pond (1982), Zeng et al. (1998)
ECMWF	$z_{0m} = 0.018\frac{u_*^2}{g} + \frac{1.65 \times 10^{-6}}{u_*}$	$z_{0h} = \frac{6 \times 10^{-6}}{u_*}$	$z_{0q} = \frac{9.3 \times 10^{-6}}{u_*}$	Beljaars (1995), Zeng et al. (1998)
NCEP	$z_{0m} = 0.014\frac{u_*^2}{g}$	$\ln\frac{z_{0m}}{z_{0h}} = \ln\frac{z_{0m}}{z_{0q}} = \frac{-1.076 + 0.7045\ln(Re_*) - 0.05808(lnRe_*)^2}{1 - 0.1954\ln(Re_*) + 0.009999(lnRe_*)^2}$		Zeng et al. (1998)
GEOS	——	$\ln\frac{z_{0m}}{z_{0h}} = \ln\frac{z_{0m}}{z_{0q}} = 0.72(Re_*{-}0.135)^{0.25}$		Zeng et al. (1998)
VM	$\log_{10}(z_{0m}) = a_m + b_m\log_{10}(u_*^2/g)$, $a_m = -1.52$; $b_m = 1.4$	$z_{0h} = \frac{z_{0m}}{\exp\{a_h + b_h\log_{10}(Re_*)\}}$, $a_h = 0.38$; $b_h = 2.99 z_{0q} = \frac{z_{0m}}{\exp\{a_q + b_q\log_{10}(Re_*)\}}$, $a_q = 2.67$; $b_q = 2.6$		Vickers and Mahrt (2010)

Notes: P1: $\alpha = 0.013$; $R_r = 0.11$ are "oceanic parameters"; P2: $\alpha = 0.031$; $R_r = 0.54$ are "optimized parameters".

3.3. Lake energy budget components

The energy budget of a lake indicates that the energy storage (G_s, Wm^{-2}) in the water is balanced by the incoming energy and the outgoing energy, and it could be simply expressed by equation (4):

$$R_n = G_s + G_b + G_a + H + LE \quad (4)$$

where R_n (Wm^{-2}; $= (1-a)R_{s\downarrow} + R_{l\downarrow} - R_{l\uparrow}$, with $R_{l\uparrow} = \varepsilon\sigma T_s^4$, $\varepsilon = 0.98$ and $a = 0.055$ are the emissivity and albedo of the water, respectively, and σ is Stefan Boltzmann constant) is the net radiation and expressed as the sum of downward short-wave radiation ($R_{s\downarrow}$, Wm^{-2}), downward long-wave radiation ($R_{l\downarrow}$, Wm^{-2}), reflected short-wave radiation ($R_{s\uparrow} = aR_{s\downarrow}$, Wm^{-2}) and long-wave radiation emitted by the water ($R_{l\uparrow}$, Wm^{-2}). G_b (Wm^{-2}) is the heat transfer between water and bottom sediments and G_a (Wm^{-2}) is the net energy gained or lost by the lake due to the exchange of water masses resulting from the inflow-outflow balance. H (Wm^{-2}) and LE (Wm^{-2}) are the sensible heat and latent heat, respectively, exchanged between the lake and atmosphere. In this study, R_n is estimated by radiation observation and T_s (°C), while G_s is estimated by temperature gradient observations. H and LE are obtained through EC observations and bulk transfer method simulations. G_b and G_a are just omitted in the calculation due to data limitations and the induced uncertainties are discussed in the Discussions. More details about the heat storage change in the water and the bulk transfer method can be found in the Supplemental Material.

4. Results

4.1. Meteorological conditions

Based on the PBL tower measurements from 2007 to 2012 in the Nam-Co station, the annual mean air temperature is approximately 0 °C, and the annual mean wind speed at a height of 10 m is approximately 4.8 m s^{-1}. However, they are approximately 1.9 °C and 5.4 m s^{-1}, respectively, in the "large lake" according to AWS observations at 9.52 m above the island in 2016 (Fig. 2c and d). The multi-year (2007–2011) average precipitation at the Nam-Co station is approximately 505 mm (Zhou et al., 2013), but it is only approximately 300 mm in the "large lake" in 2016 (Fig. 2b). The largest short-wave radiation reached to 1250 W m^{-2}, which is much higher than that in low-elevation lakes (Fig. 2a) and higher than that in the high-elevation Lake Ngoring (Li et al., 2015a). The wind direction in the "large lake" favors the southwest, with a peak frequency of 220° (Fig. 1c3), while the wind direction in the "small lake" area is more scattered, concentrating to the south and southwest (Fig. 1b3). The observed sensible heat flux and latent heat flux after quality control show quite similar variations with the simulated results using the bulk transfer method (Fig. 2e and 2f), which will be discussed in detail in Section 4.3. In November 2016, we also observed Secchi depths of the water, with values of 6 m and 2.8 m for the "large lake" and the "small lake", respectively. Thus, the "large lake" is more transparent to solar radiation than the "small lake".

The field observations in the "small lake" and "large lake" are conducted during 2012–2013 and 2015–2016, respectively. Thus, to justify the results of the comparison of these two water bodies, we first quantitatively compared the seasonal variations of meteorological variables at a height of 10 m in the Nam-Co station during the two periods, with multi-year (2006–2016) average as the climatic background (Fig. 3). The seasonal variations of the meteorological variables are quite similar between 2012 and 2013 and 2015–2016, especially during the open water periods. The averaged downward short-wave radiation, air temperature, relative humidity and wind speed are 242.7 W m^{-2}, −0.14 °C, 48.0% and 4.99 m s^{-1} during 2012–2013 while those values are 245.7 W m^{-2}, 0.29 °C, 46.7% and 4.78 m s^{-1} during 2015–2016. The most significant differences could be found in downward short-wave radiation during July, where a much higher value exists in 2015–2016 than that found in 2012–2013 (Fig. 3d). These differences result from the fact that continuous clear day exist in July 2015. Thus, cloud cover during the monsoon season, which also contribute to the observed large uncertainties, explains most of the variabilities. Except for this discrepancy, all other meteorological variables generally are located closely to the multi-year averages and lay in the ranges of their uncertainties. Thus, the macro driving meteorological variables during periods of 2012–2013 and 2015–2016 show no significant differences, and the significant differences existing between the two water bodies should result from their inherent attributes and environmental differences, rather than the climatic variability.

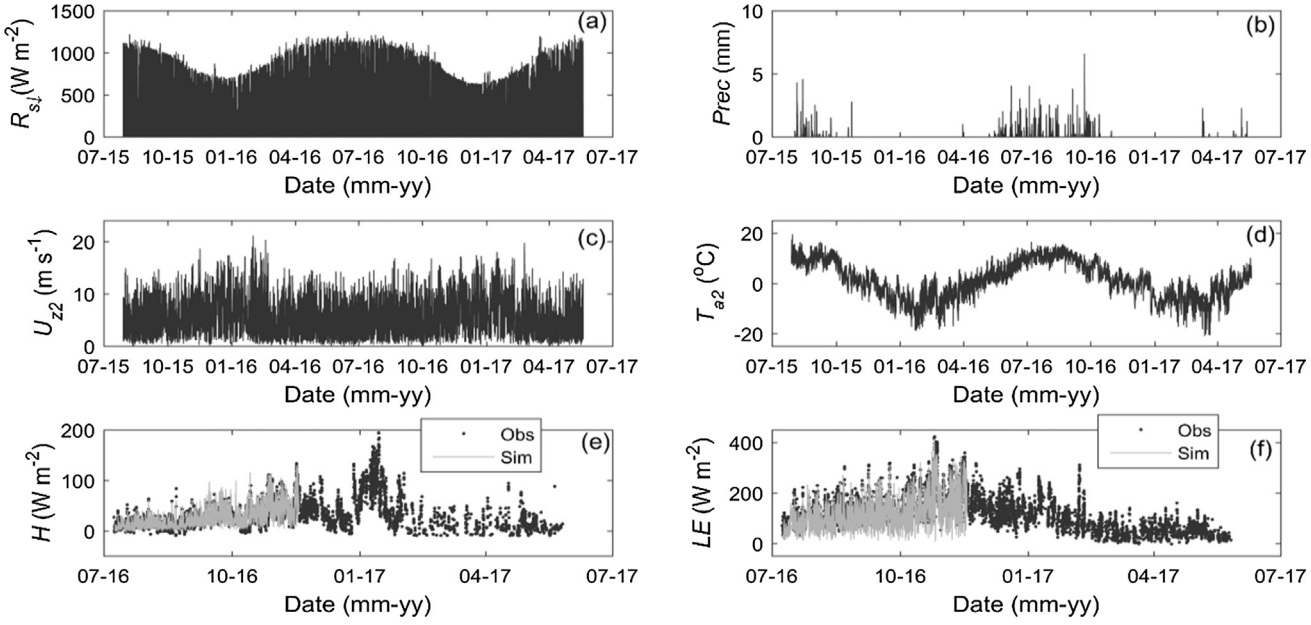

Fig. 2. Variation of half-hour (a) downward short-wave radiation ($R_{s\downarrow}$), (b) precipitation (Prec), (c) U_{z2} (wind speed at a height of 9.52 m), (d) T_{a2}(air temperature at a height of 9.52 m), (e) H, and (f) LE during their observational periods in the "large lake". "Obs" indicates the observed H and LE after quality control and "Sim" indicates the simulated H and LE by the bulk transfer method.

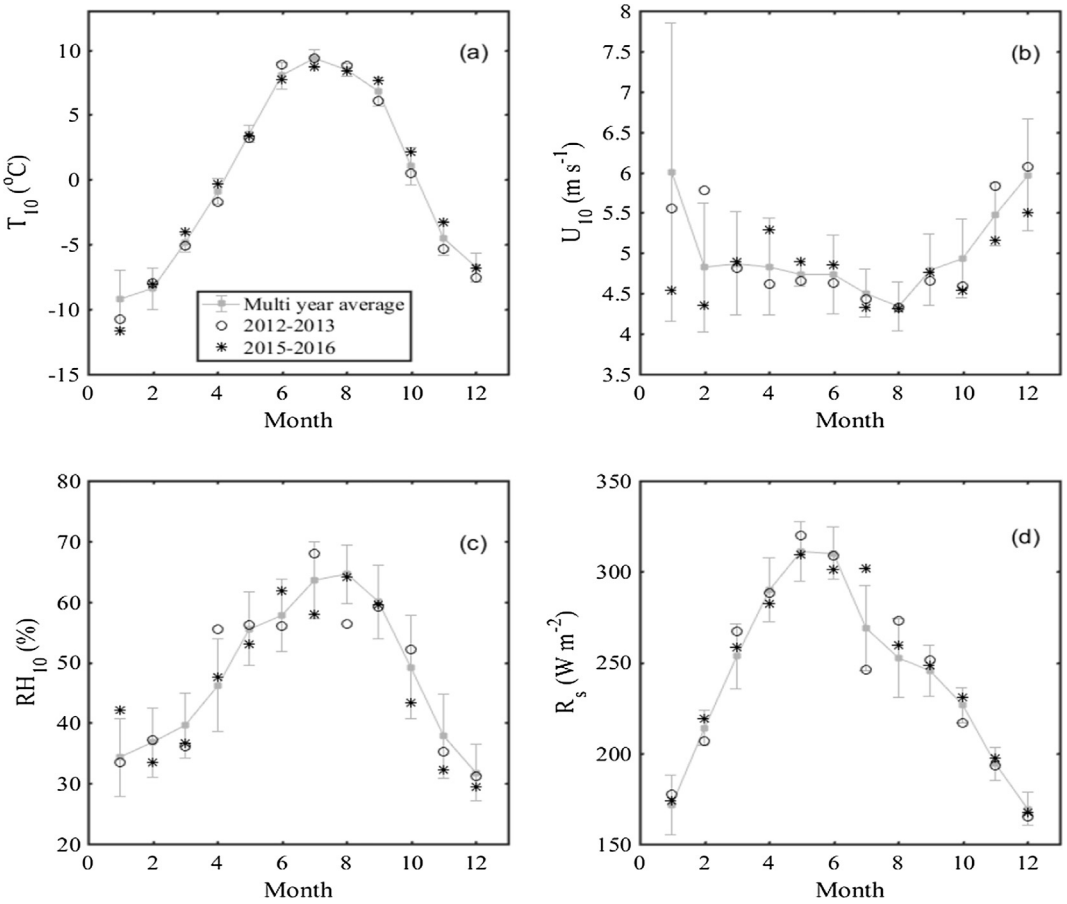

Fig. 3. Comparison of monthly averaged meteorological variables of (a) T_{10}, (b) U_{10}, (c) RH_{10} and (d) R_s for the period of the "small lake" (2012–2013, circle), and the period of the "large lake" (2015–2016, star). The multi-year average (2006–2015) of meteorological variables with error-bars are also marked.

4.2. Comparison of boundary layer parameters

4.2.1. Comparison of roughness lengths

The typical value of momentum roughness length (z_{0m}) in the "small lake" has been reported to be 3.35×10^{-4}m (Wang et al., 2015) while the value in the "large lake" is 80% higher (6.11×10^{-4}m) (Fig. 4a). z_{0m} in the "large lake" is quite close to the reported value (6.17×10^{-4}m) in another high-elevation lake of Lake Ngoring (Li et al., 2015b), with an area of 610 km^2. The relatively higher z_{0m} in the "large lake" than in the "small lake" results from the higher wind speed and larger wind-induced waves. Moreover, as shown in Fig. 4a and 4b, the optimized parameters (P2, $\alpha = 0.031$ & Rr = 0.54 in UA method in Table 2) both in the "small lake" and in the "large lake" are more appropriate for momentum roughness length estimation than the oceanic parameters (P1, $\alpha = 0.013$ & Rr = 0.11). The parameterization scheme with a combination of rough flow (α) and smooth flow (Rr) could improve z_{0m} at large u_* and small u_*, respectively. Thus, the combined form with optimized parameters (P2) not only shows better performance than the forms (e.g., UA and ECMWF) with oceanic parameters but also performs better than the forms with only single item (e.g., NCEP, not shown in Fig. 4). The scheme of VM shows significant underestimation. Thus, the parameter scheme of the combined form with optimized parameters will be used for z_{0m} simulation in the "large lake".

The peak of the distribution of z_{0h} is much larger in the "small lake" than in the "large lake", especially in the range of strong wind (Fig. 4c and 4d and Fig. 5b). The typical value of z_{0h}, 3.35×10^{-4}m in the "small lake", is one order of magnitude higher than that (1.67×10^{-5}m) in the "large lake" (Fig. 4b). z_{0h} in the "large lake" is at same order of magnitude as the value (7.59×10^{-5}m) in Lake Ngoring (Li et al., 2015b) and it is also close to the values from CCM3 and ECMWF (Table 2). The parameterization scheme of UA for z_{0h} is more suitable for the "small lake" than for the "large lake". The parameterization schemes of GEOS and VM are quite similar to that of UA, with slightly lower value of the GEOS scheme in ranges of small u_* and slightly lower value of the VM scheme in ranges of large u_*. The parameterization scheme of NCEP shows an overestimation of z_{0h}. All these parameterization schemes of z_{0h} are much more suitable in the "small lake", but have an obvious overestimation in the "large lake". Because the parameterization scheme of UA shows similar variation to the observations, the UA form is optimized (constant value changing from -2.57 to -0.57) for the sensible heat flux simulation in the "large lake".

Similarly, the typical z_{0q} values are 3.35×10^{-4}m in the "small lake" and 5.54×10^{-5}m in the "large lake"(Fig. 4c). The latter is quite close to the observed value (6.73×10^{-5}m) in Lake Ngoring (Li et al., 2015b). The parameterization schemes of UA and GEOS show quite similar results, with the latter having lower values than the former in the range of small u_*. The parameterization scheme of NCEP is overestimated while the parameterization scheme of VM is underestimated compared to the observations (Fig. 4e and 4f). Without optimization, the good performance of the parameterization scheme of UA could be used for the latent heat flux simulation in the "large lake". In a brief conclusion, the parameterization schemes of roughness lengths for momentum, heat and water should be evaluated before being applied to the high-elevation lakes of TP, and our results could provide reference values.

4.2.2. Comparison of bulk transfer coefficients

The bulk transfer coefficients for momentum (C_{Dz}) at observational heights of 2.75 m and 6 m are same (0.002) in the "small lake" and the "large lake", while the coefficients (C_{DN10}) corrected to a reference height of 10 m and neutral conditions are 0.0014 and 0.0017,

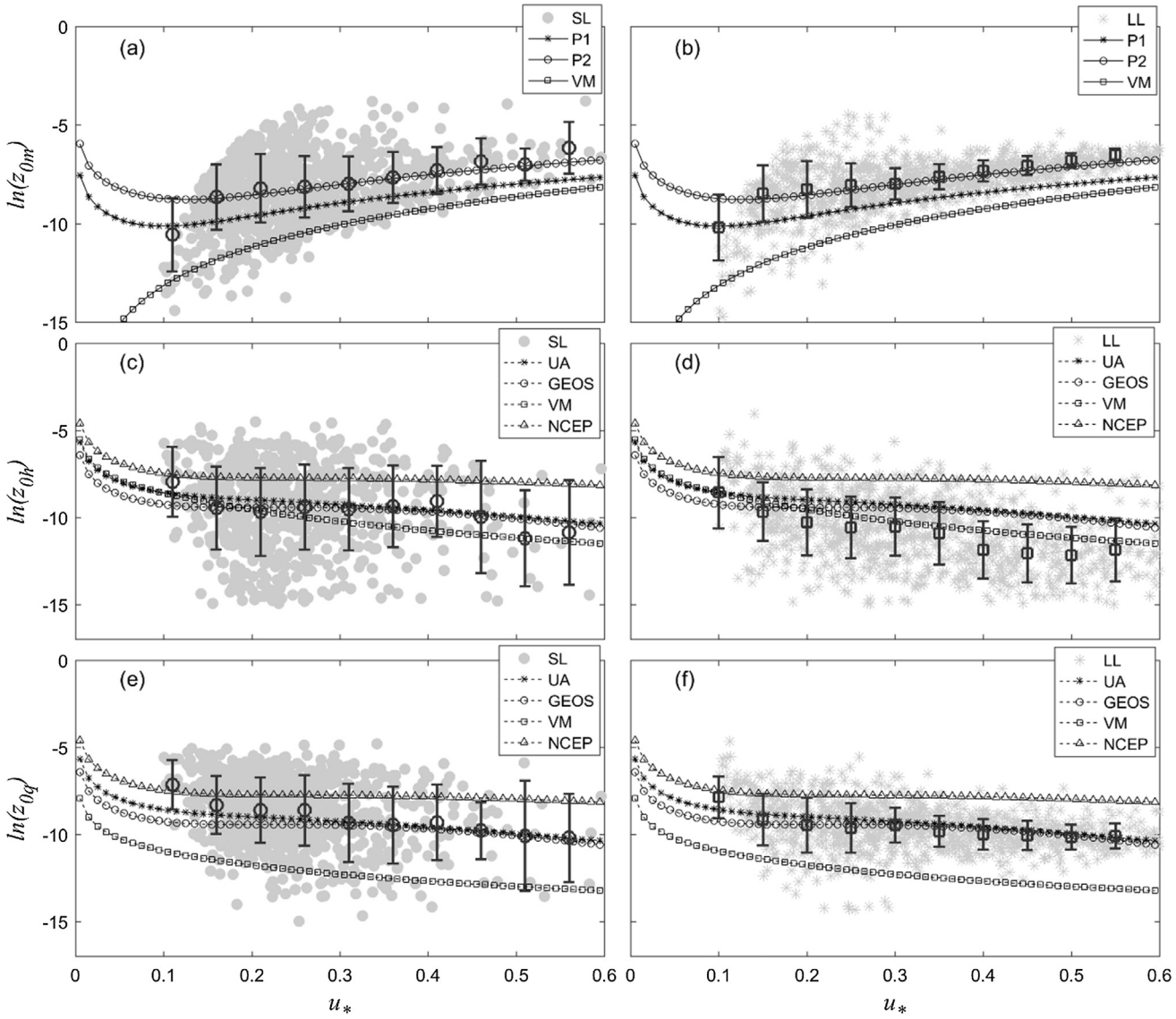

Fig. 4. Comparison of roughness lengths for (a)-(b) momentum, (c)-(d) heat and (e)-(f) water and evaluation of the parameterization schemes in the "small lake" and the "large lake" respectively. "SL" indicates the observed roughness lengths in the "small lake", "LL" indicates the observed roughness lengths in the "large lake", the circles and the squares are the mean of observations for each binned u_* in the "small lake" and the "large lake", respectively (from 0.05 to 0.6 with a bin size of 0.05, error bars are marked) and the lines indicate all kinds of parameterization schemes.

respectively (Fig. 5d). The larger C_{DN10} in the "large lake" may result from the combined effects of larger wind-induced waves and complex basin environments (i.e., huge stones in the water). The C_{DN10} in the "small lake" (0.0014) is quite close to the value (0.00149) in the leads and polynyas of polar oceans (Andreas and Murphy, 1986), with both higher than the reported open-ocean values of approximately 0.0012 at a medium range of wind speed (Large and Pond, 1981). Because of the limited wind fetch, the upwind edges of grassland and the growing wave field in the "small lake" may attribute to the larger form drag than the open oceans. However, the even larger C_{DN10} (0.0017) in the "large lake" than in the "small lake" could only be ascribed to its large wind-induced waves (Wu, 1980).

The bulk transfer coefficients for heat (C_{HN10}) at a height of 10 m and neutral conditions are 0.0014 and 0.0013 (Fig. 5e) in the "small lake" and the "large lake" while the bulk transfer coefficients for water (C_{EN10}) are 0.0015 and 0.0014, respectively (Fig. 5f). These coefficients are approximately 7% lower in the "large lake". These estimated C_{HN10} and C_{EN10} are all larger than the published typical oceanic value of 0.0012 (Smith, 1989; Zeng et al., 1998). The larger scatter in the range of small u_* (Fig. 4) in the "small lake" than in the "large lake" may result from the relative higher measurement uncertainties under free convection events, which indicates the dominance of buoyancy over shear and happens more often in the "small lake" area.

4.3. Turbulent heat flux simulation in the "large lake"

The bulk transfer method with optimized roughness lengths (z_{0m}, z_{0h}, z_{0q}) is used for simulation of the lake-air turbulent heat flux in the "large lake", and the simulations show quite similar results compared with EC observations chosen by the criteria of footprint and data quality control (Fig. 6a–c). The RMSE values of H and LE are only approximately 10 W m^{-2} and 30.2 W m^{-2}, and the correlation coefficients are 0.90 and 0.91, both as good as those in the "small lake" (Wang et al., 2015, 2017). The seasonal variations of monthly averaged H, LE and u_* between simulations and observations are quite consistent, with a small bias of monthly averaged MB values (Fig. 6d–f). The relatively higher MB values of H appear in November during a period when the H values are larger. The averaged MB values of H and LE

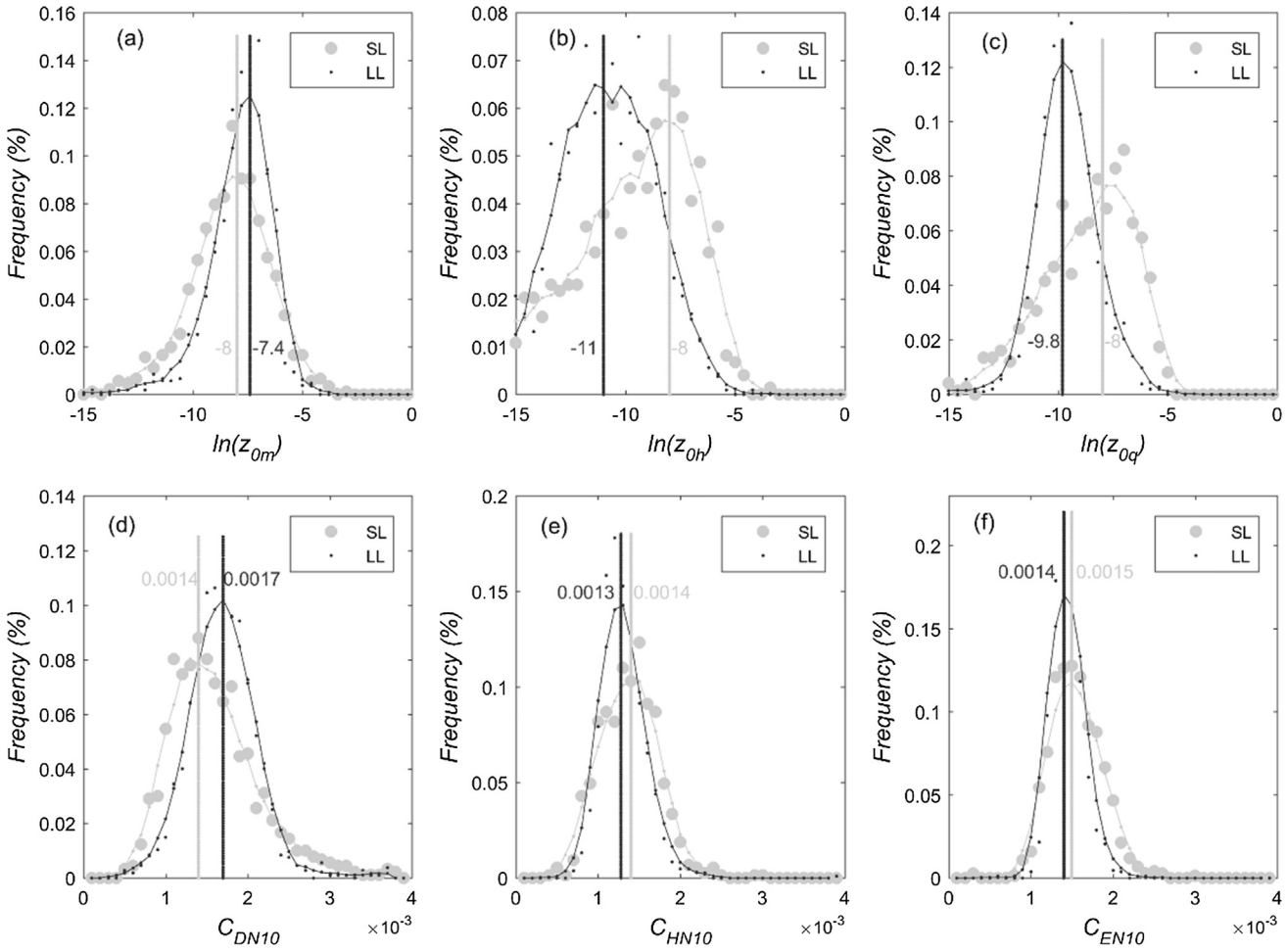

Fig. 5. Statistical distributions of logarithm forms of (a) roughness length for momentum ($ln(z_{0m})$), (b) roughness length for heat ($ln(z_{0h})$), (c) roughness length for water vapor ($ln(z_{0q})$), (d) bulk transfer coefficient for momentum, (e) bulk transfer coefficient for heat, and (f) bulk transfer coefficient for water vapor. "SL" indicates the smoothed values in the "small lake" and "LL" indicates the smoothed values in the "large lake". The values are also marked on each figure.

during the observational periods are only 3.7 W m^{-2} and −2.8 W m^{-2}, respectively, corresponding to a small overestimation of H and a minor underestimation of LE. The friction velocity (u_*) between simulation and observation also has quite a high correlation coefficient (R = 0.87) and good slope values close to the 1:1 line (Fig. 6c–f). Thus, the bulk transfer method could simulate the lake-air turbulent flux at a temporal resolution of a half-hour, and EC observations with bad quality and an inadequate footprint could be substituted by simulations of the bulk transfer method. The constructed continuous data series are further used for the comparative analysis of seasonal variation of the turbulent heat flux, evaporation and energy budget in the "small lake" (Wang et al., 2017) and in the "large lake".

The environmental controls on the turbulent heat flux over temporal scales of half-hour and daily in the "small lake" are summarized in Wang et al. (2017), and the results for the "large lake" are listed in Table 4. At the half-hour scale, the correlation coefficients from high to low are $U_z\Delta E$, U_z and ΔE for LE and $U_z\Delta T$, U_z, ΔT for H in the "small lake". Quite similarly, the correlation coefficients are 0.93 ($U_z\Delta E$), 0.81 (U_z) and 0.34 (ΔE) for LE and 0.77 ($U_z\Delta T$), 0.66 (ΔT) and 0.23 (U_z) for H in the "large lake". Atmosphere stability (ζ) shows weak correlation in both lakes. Thus, it could be inferred that U_z is the most significant factor in the simulation of half-hour evaporation in lakes on the TP, and it has also been confirmed by the high-elevation lakes of Lake Qinghai (Li et al., 2016) and Lake Serling (Guo et al., 2016). When the relative contributions of environmental factors are analysed on a daily scale, all the correlation coefficients increased, especially for ΔE (0.34 to 0.66 in Table 3). As U_z and LE in the "large lake" both show increasing trends from July to November, their correlation coefficients should be higher than those in the "small lake", where the wind speed has no obvious pattern during its ice-free seasons.

4.4. Comparison of meteorological variables and turbulent heat flux

The seasonal variations of in situ meteorological variables and turbulent heat flux during the observational periods of 2015 and 2016 in the "large lake" are shown in Fig. 7, and details of those in the "small lake" can be found in Wang et al. (2017). Furthermore, the monthly averages of the above observations have also been summarized in Fig. 8 for comparison. Similar to the "small lake", daily T_a and E_a are generally smaller than daily T_s and E_s in the "large lake", especially during the cooling period (Fig. 7a and 7b). Daily water surface temperature (T_s) could be approximately 13 °C at the beginning of September in the "large lake" (12.3 °C on September 9, 2015 and 12.9 °C on September 2, 2016 in Fig. 7a) while it could reach approximately 16 °C during the middle of June (15.7 °C on June 15, 2012 and 15.9 °C on June 21, 2013) in the "small lake". The average wind speed (corrected to a reference height of 10 m) is approximately 3.65 m s^{-1} during July through November in the "small lake", while it is 4.71 m s^{-1} (corrected at a reference height of 10 m) in the "large lake" (Fig. 7c). Thus, there were clearly higher wind speeds in the "large lake" than those in the "small lake" (Fig. 8c). Similar to the "small lake", an unstable atmosphere also dominates in the "large lake" (Fig. 7d). The vapor pressures of air in

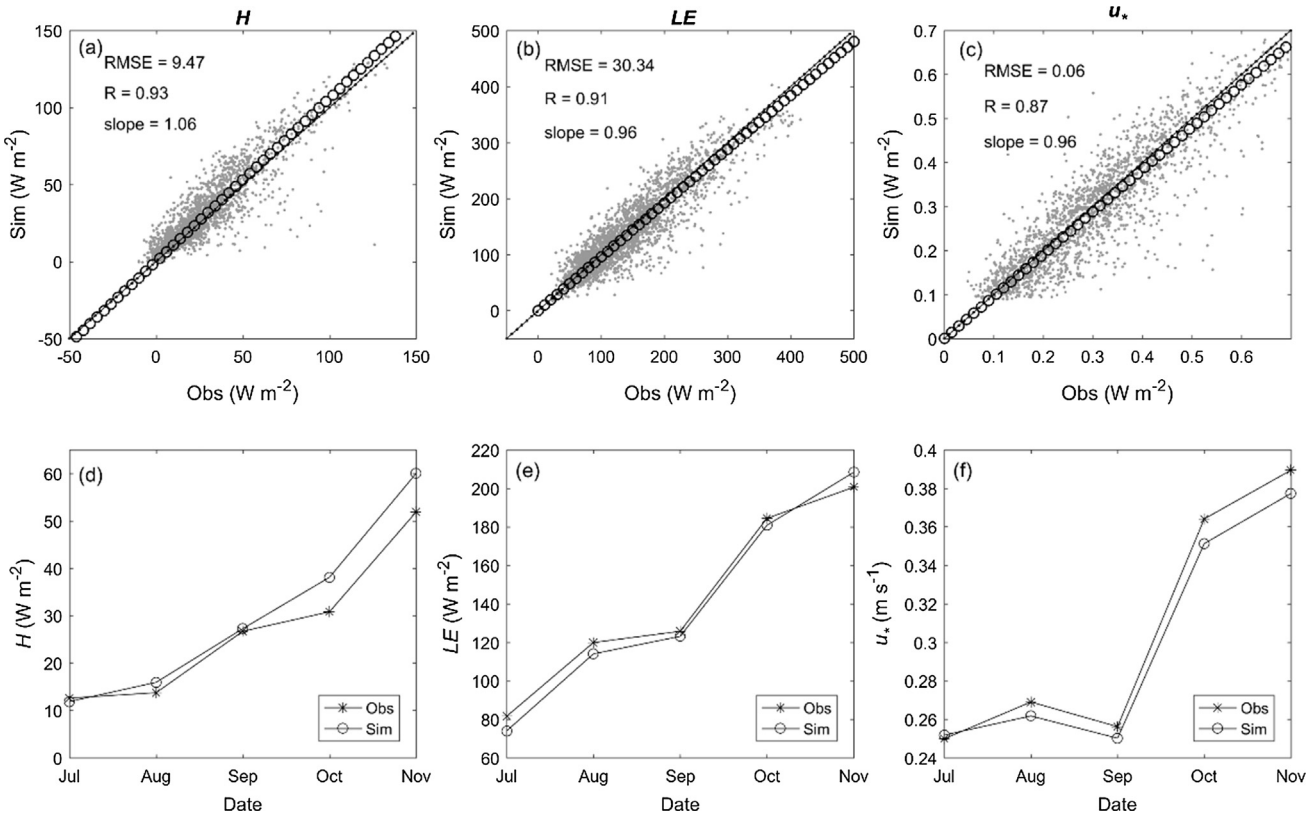

Fig. 6. Scatterplots of (a) *H*; (b) *LE;* and (c) u_* between bulk transfer method simulations (Sim) and observations (Obs) in 2016 (lines drawn with dots and circles represent the1:1 line and the line of best fit, respectively; correlation coefficients (R) and the slope of the line of best fit (passing through the origin) are marked) and the monthly average values of (d) *H*; (e) *LE;* and (f)u_* between simulated and observed results for each month.

Table 4
Correlation coefficients (R) between *H* & *LE* and environmental variables of the "large lake" from July to November in 2016.

Variables	Temporal scales	(R)	Variables	Temporal scales	(R)
$H\sim U_z$	30 Minutes	0.23	$LE\sim U_z$	30 Min	0.81
	Daily	0.48		Daily	0.81
$H\sim \Delta T$	30 Minutes	0.66	$LE\sim \Delta E$	30 Min	0.34
	Daily	0.84		Daily	0.66
$H\sim U_z\Delta T$	30 Minutes	0.77	$LE\sim U_z\Delta E$	30 Min	0.93
	Daily	0.99		Daily	0.98
$H\sim \zeta$	30 Minutes	−0.15	$LE\sim \zeta$	30 Min	0.22
	Daily	0.18		Daily	0.43

both lakes reach their highest values in July and then decrease afterwards (Fig. 8d). Because of the relatively higher wind speed and lower T_s in the "large lake", the atmosphere was less unstable compared with that in the "small lake". Moreover, because of the strong "warm lake effect" in the "large lake" (Lv, 2008), the average air temperature (1.9 °C) in 2016 is obviously higher in the "large lake", compared with multiple year average of air temperature (approximately 0 °C) in the Nam-Co station. Moreover, the monthly average air temperature (T_a) is clearly higher in the "large lake" than that in the "small lake" (Fig. 8b). Relative to the "small lake", the large thermal capacity in the "large lake" could also lead to a late date of the peak value of monthly T_s, a slow decreasing rate of T_s (Fig. 8a) and thus late dates of ice-frozen and ice-melt. In addition, monthly average T_a decreases much slower in the "large lake" (Fig. 8b).

Daily *H* and daily *LE* in the "large lake" both show increasing trends from July to November (Fig. 8g and h), while the daily ΔT and daily ΔE between the water and air also show increasing trends (Fig. 8e and f) at the same time, in addition to the clearly increasing trend of daily U_z from September to November (Fig. 8c). The variation of daily *H* is similar to that of daily ΔT, while the variation of daily *LE* is more similar to daily U_z than daily ΔE. For example, in October 2015, high daily ΔE and low daily *LE* exist (Fig. 7f–h). The relative contributions of meteorological variables to the turbulent heat flux can be seen in Table 4 and Section 4.3. Influenced by the large thermal capacity of the "large lake" and the strong land-lake breeze circulation, the monthly averaged ΔT is much higher in the "small lake" than in the "large lake" (Fig. 8e). Thus, the monthly averaged *H* values are generally higher in the "small lake" than those in the "large lake", except in November, when the significantly high U_z in the "large lake" has a dominant contribution (Fig. 8c-e-g). Variations of monthly *LE* and monthly ΔE show quite different patterns in the two lakes, and they are higher for July and August and lower for October and November in the "small lake" compared to those in the "large lake" (Fig. 8f–h).

4.5. Energy budget and evaporation in the "large lake"

The radiation budget components and net radiation (R_n) during the observational periods are shown in Fig. 9, and the energy budget components, including meteorological variables, are summarized in Table 5. The R_n peaked in July while *LE* peaked in November; thus, *LE* shows an approximately 4-month lag of R_n. The mean temperature of the whole water column ($\bar{T}_w$) shows largest value in September, which is also the turning point from heat storage to heat release in the "large lake", while it is around August in the "small lake" (Wang et al., 2017). The seasonal variation of *LE* in the "large lake" by Flake simulations (Lazhu et al., 2016) also shows an increasing trend from summer to autumn, but the largest value appears in October, which is one month earlier than the observations. During July to November, the Bowen ratio ($Bo = \frac{H}{LE}$) in the "large lake" shows an increasing trend from 0.139 to 0.298, with an average value of approximately 0.229, which is generally smaller than the average value (Bo = 0.333) in the "small

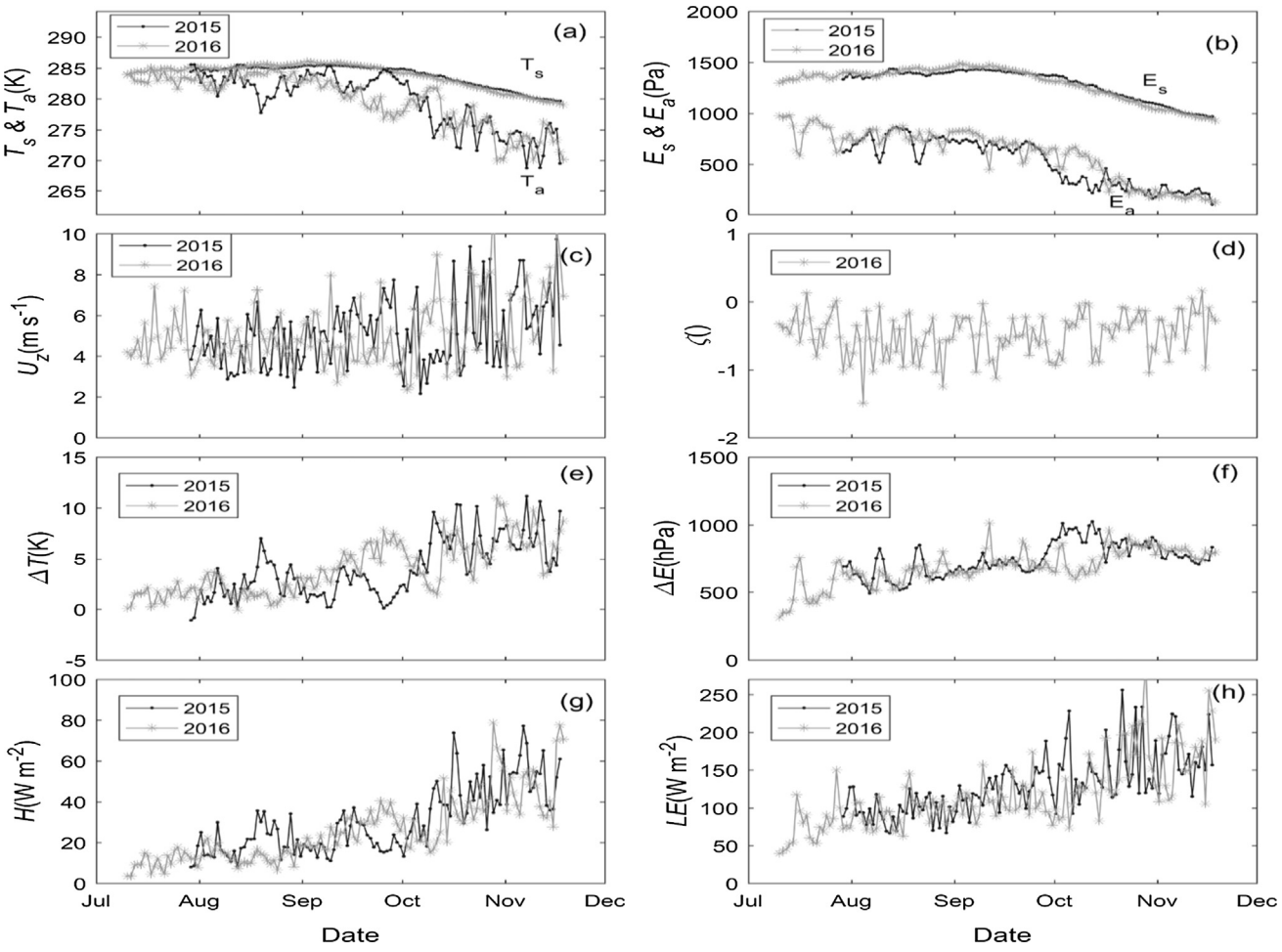

Fig. 7. Variation of daily (a) T_s & T_a; (b) E_s & E_a; (c) U_z; (d) ζ; (e) ΔT; (f) ΔE, (g) H, and (h) LE during July to November in 2015 and 2016.

lake" during the same months (Wang et al., 2017). Assuming the heat budget is balanced during July to November, the balance of monthly R_n, monthly LE and monthly H is $-8.6\,W\,m^{-2}$, which corresponds to the heat release of the "large lake", with $\bar{T_w}$ decreasing from 8.3 °C to 6.9 °C. The higher Bowen ratios ($Bo = \gamma\frac{(T_s - T_a)}{(E_s - E_a)}$) could also be explained by the meteorological observations of higher temperature gradients and nearly similar water vapor gradients in the "small lake" than in the "large lake" (Fig. 8e and f). The energy budget closure ratio ($EBC = \frac{H+LE}{R_n - G}$) ranges from 0.647 in July to 1.308 in August, with an average value of 0.859 from July to November.

Compared with evaporation in the "small lake", the observed values in the "large lake" are smaller during July to September and are larger during October and November. The observed total evaporation in the "large lake" is approximately 630 mm from July to November. The total evaporation in the ice-free season of the "small lake" is approximately 812 mm (Wang et al., 2017). To obtain the total evaporation of the "large lake", we made a reasonable hypothesis that the heat stored in the water after ice-out could all be released before ice-formation; thus, the evaporation could be determined by R_n and Bo. Table 6 shows the radiation budget components of the "large lake" in 2016, where $R_{s\downarrow}$ and $R_{l\downarrow}$ come from radiation observations on the island while $R_{l\uparrow}$ is estimated by lake surface temperature (average value of all pixels in the lake area) from MODIS products (MOD11A2 and MYD11A2), which contain both day and night products at a spatial resolution of 1km × 1km. First, R_n is highest in June and lowest in December, with all the values being positive. The positive R_n corresponds to the observed positive LE and H, even during the ice-covered period (Fig. 2e–f). Second, the $R_{l\uparrow}$ estimated by MODIS land surface temperature products has a mean bias of $-5\,W\,m^{-2}$ compared with $R_{l\uparrow}$ derived using the water surface temperature, and they are quite close after bias correction, as shown in Fig. 9c. Last, the total R_n from May to January is 1164 Wm^{-2}; thus, the evaporation during the open water period of the "large lake" is approximately 981 ± 18 mm, assuming a Bo of 0.229 with an uncertainty of 10%.

5. Discussion

5.1. The causes of the observed differences in the meteorological variables

The inherent attributes and environmental backgrounds of the two adjacent water bodies could explain most of the observed differences. (i) The higher wind speed in the "large lake" may result from its lake-dominated environment with the footprint of smooth water, compared with the land-dominated "small lake" area influenced by the surrounding grassland (Granger and Hedstrom, 2011). In addition, the bowl-shaped terrain of the "small lake" may form specific internal boundary layer conditions different from those of the "large lake". (ii) The maximum daily T_s in summer can be approximately 3 °C lower in the "large lake" than in the "small lake" (Fig. 8a), and the reason is that the solar heating could be distributed to deeper depths in the "large lake" than in the "small lake". More specifically, the "large lake" has the characteristics of (1) a larger Secchi depth, allowing it to be more transparent to solar radiation and to store more heat in the deep water (Heiskanen et al., 2015); (2) a stronger turbulence exchange intensity, making it easier to transfer heat into deep water; (3) a deeper depth, resulting in a higher potential for storing heat. (iii) Because of the larger

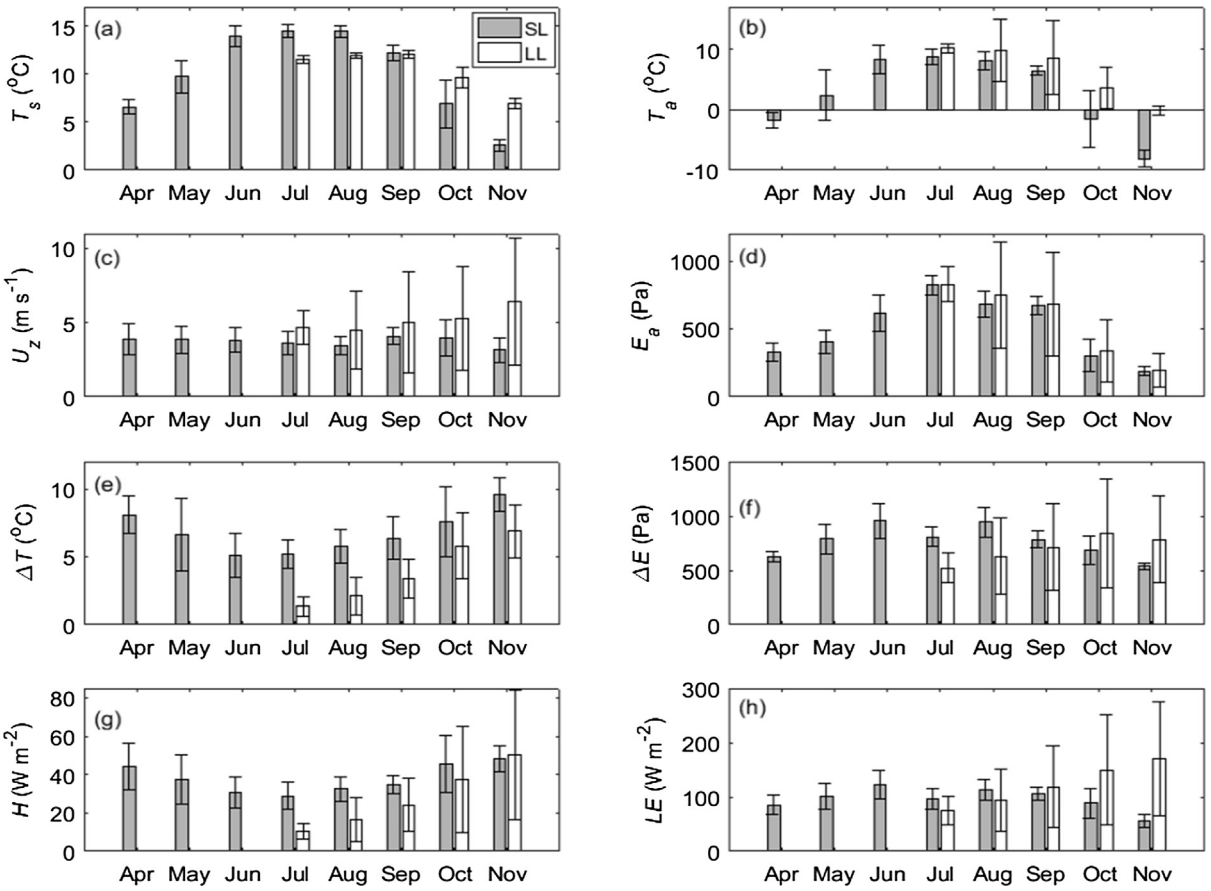

Fig. 8. Comparison of (a) water surface temperature (T_s), (b) air temperature (T_a), (c) wind speed (U_z), (d) vapor pressure of the air (E_a), (e) temperature gradients (ΔT), (f) water vapor gradients (ΔE), (g) H, and (h) LE between the "small lake" (SL) and the "large lake" (LL).

heat capacity in the "large lake", the phenomenon of warm air temperature, a slow decrease of air temperature in autumn, and delayed peaks of seasonal H and LE exist. (iv) The precipitation of approximately 300 mm in the lake-dominated environment in 2016 is much smaller than the climatic average of the land-dominated environment of the "small lake", which is mainly driven by the land breeze and land surface interaction; thus "small lake" may have higher precipitation than the lake-dominated environment (Gerken et al., 2015). (v) The highest value of LE appears in November in the "large lake", while the peak appears in August in the Lake Ngoring (Li et al., 2015a) and in June in the "small lake". The difference results from the larger heat storage in the water of the "large lake", which could provide an energy supply and lead to a phase shift of LE. Thus, even in regions with the same climatic conditions, the meteorological variables and turbulent heat fluxes of different water bodies show significant differences in their seasonal variations. (vi) Similar as those low-latitude tropical lakes (Verburg and Antenucci, 2010), high-elevation lakes show dominance in unstable and neutral atmospheric conditions in these two lakes and some other lakes, i.e., Lake Qinghai (Li et al., 2016), Lake Serling Co (Guo et al., 2016), and Lake Ngoring (Li et al., 2015). The unstable atmosphere conditions in high-elevation lakes and tropical lakes result from the higher solar radiation and radiation-induced positive water–air temperature gradients compared to the temperate low-elevation lakes. More discussion on influences of these characteristics to turbulent heat fluxes could resort to Verburg and Antenucci (2010).

5.2. The uncertainties in evaporations and its influence

The EC-based evaporation in the "large lake" (630 mm during July to November) is much higher than the reported value (392 mm) in Lake Ngoring during July to November (Li et al., 2015a), and the amounts of R_n, 169.5 W m^{-2} higher in the "large lake", could explain most of the differences. The estimated evaporation during May to January (approximately 981 ± 18 mm) of the "large lake" is also higher than the simulated results from the Flake model (Lazhu et al., 2016) and the CRLE model (Ma et al., 2016). Both the uncertainties in the input meteorological data and the unsuitable parameterization schemes of the models could lead to such bias, and our results could provide valuable data for future validation and evaluation of these models. The ratio of evaporation (981 ± 18) to rainfall (505 mm) is 1.9 in this study, while they are 3.5 (with evaporation and precipitation values of 1430 mm and 420 mm, respectively) in Zhu et al. (2010) and 1.2 (with evaporation and precipitation values of 603 mm and 505 mm, respectively) in Zhou et al. (2013). Zhu et al. (2010) conclude that underground water or other sources are needed to complement the huge evaporation, while Zhou et al. (2013) suggest that water seepage exists. Except for the other differences in their estimated precipitation and runoff values and runoff coefficients, the EC-based evaporation value of 981 ± 18 mm could improve the understanding of their conclusions in a water imbalance analysis.

The uncertainties in the estimated evaporation of 981 ± 18 mm should result from the uncertainties existing in Bo and R_n. First, assuming the heat stored in the water after ice-melt will all be released before ice-frozen, LE could be expressed as $LE = \frac{R_n}{(1+Bo)}$. Thus, lake evaporation is positive correlated with R_n and negative correlated with Bo. The sum of R_n during the open water period of the "small lake" (with a value of 1167.9 W m^{-2} in Table 4 of Wang et al. (2017) is quite close to the sum of R_n during the open water period of the "large lake" (1164 W m^{-2} in Table 6). The estimated lower Bo in the "large lake" than in the "small lake" indicate a higher evaporation value in the

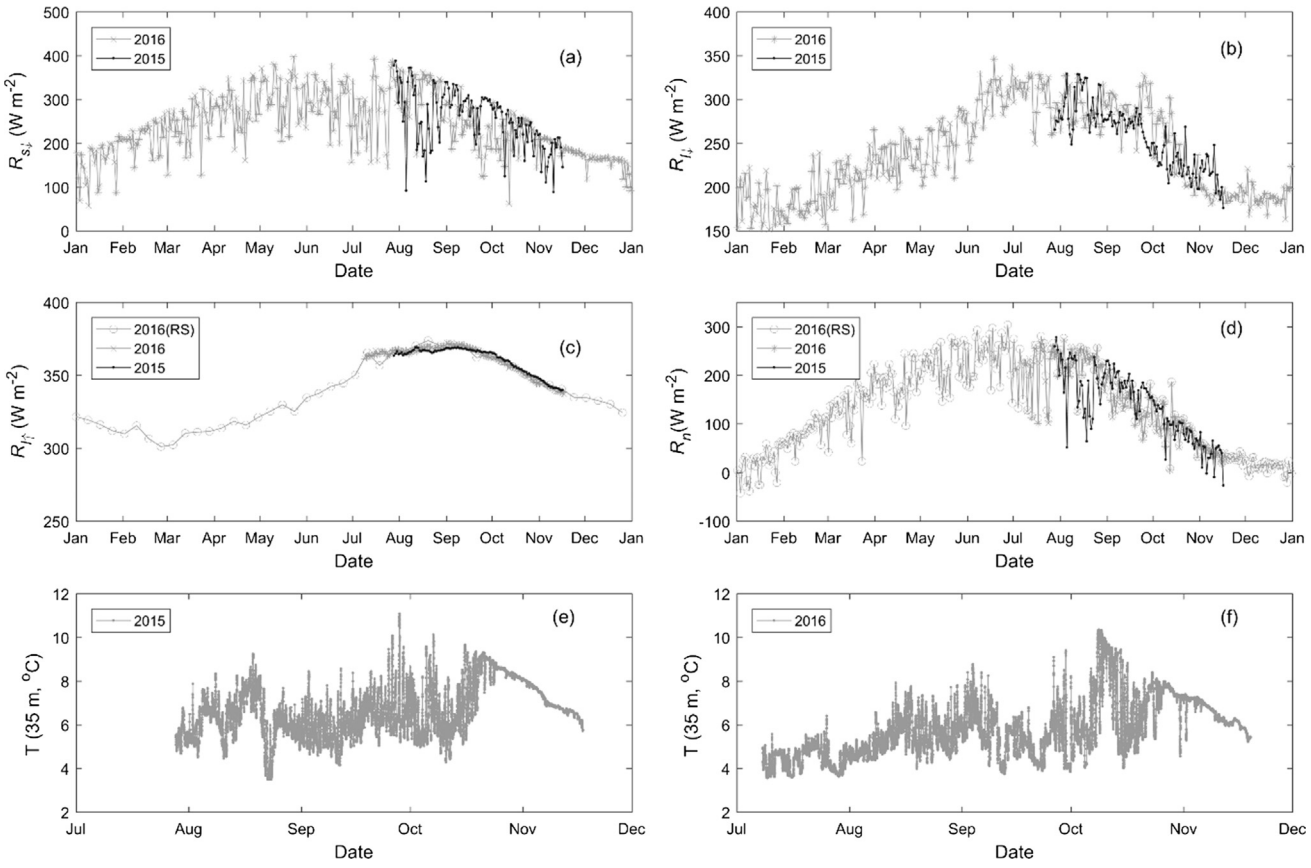

Fig. 9. Variation of daily (a) downward short-wave radiation ($R_{s\downarrow}$); (b) downward long-wave radiation ($R_{l\downarrow}$); (c) upward long-wave radiation ($R_{l\uparrow}$); (d) net radiation (R_n) in 2015 and 2016; (e) water temperature at a depth of 35 m in 2015; and (f) water temperature at a depth of 35 m in 2016. "2016(RS)" indicates the MODIS products.

Table 5
Monthly averaged environmental variables and heat fluxes during the open-water period of the "large lake" in 2015 and 2016. "Ave" indicates average values of 2015 and 2016 while and "*Ave*" indicates averages of variables from July to November (August to November in 2015).

Variables	Year	July	August	September	October	November	$\bar{}$ Ave
$\bar{T_w}$(°C)	2015	——	9.9	10.4	9.2	7.1	9.2
	2016	8.3	9.7	10.4	8.8	6.7	8.8
	Ave	8.3	9.8	10.4	9.0	6.9	8.9
R_n(W m^{-2})	2015	——	186.0	178.8	97.3	36.6	124.7
	2016	207.6	221.7	140.1	91.8	40.0	140.3
	Ave	207.6	203.9	159.5	94.6	38.3	**140.8**
G(W m^{-2})	2015	——	115.6	1.5	−134.4	−218.0	−58.8
	2016	74.4	121.9	−31.6	−168.0	−167.0	−34.1
	Ave	74.4	118.8	−15.1	−151.2	−192.5	**−33.1**
Bo	2015	——	0.204	0.166	0.259	0.313	0.236
	2016	0.139	0.146	0.248	0.241	0.282	0.211
	Ave	0.139	0.175	0.204	0.250	0.298	**0.229**
EBC	2015	——	1.625	0.837	0.831	0.869	1.041
	2016	0.647	1.083	0.798	0.698	1.055	0.856
	Ave	0.647	1.308	0.817	0.761	0.952	**0.859**

former. Average *Bo* without consideration of its seasonal variation in this study may introduce some uncertainties. For example, a warmer air temperature than water surface temperature in the "large lake" may form during May and June according to satellite and AWS observations, similar to the observations in Lake Serling (Guo et al., 2016), and smaller *Bo* in May and June and larger *Bo* in December and January may exist. The estimated evaporation through EC-based *Bo* value of 0.229 (close to the *Bo* value in September) could only repreesnt a rough estimation.

Further, we used ice phenology to estimate the lower and upper boundaries of the open water evaporation in the "large lake". The average dates of freeze onset (FO, the date when detectable ice appears), freeze-up (FU, the date when the surface is fully ice covered), break-up (BU, the date when detectable ice-free water appears) and water clean of ice (WCI, the date when ice all disappears) are 4th January, 13th February, 4th April and 15th May, respectively by satellite observations (Kropáček et al., 2013). The duration from FU to BU is longer in three adjacent small lakes (Lake Ringco Ogma, Lake Npen Co and Lake Bam Co) relative to Lake Nam-Co. The estimated evaporation values through R_n and *Bo* are 885± 17 mm during FU to BU

Table 6
Radiation components (downward short-wave radiation ($R_{s\downarrow}$), downward long-wave radiation ($R_{l\downarrow}$), upward long-wave radiation ($R_{l\uparrow}$), net radiation (R_n)) of the "large lake" in 2016, units: Wm^{-2}.

	Jan	Feb	Mar	Apr	May	Jun	Jul	Aug	Sep	Oct	Nov	Dec
$R_{s\downarrow}$	158.3	214.2	245.0	277.1	310.0	294.8	282.6	317.5	230.6	220.5	191.1	154.8
$R_{l\downarrow}$	178.2	182.6	211.0	233.0	252.2	296.2	302.4	289.7	290.3	237.5	191.5	189.0
$R_{l\uparrow}$	311.7	308.5	310.0	316.5	328.3	347.7	362.8	371.4	366.5	352.3	337.4	326.4
R_n	16.1	76.5	132.5	178.4	216.9	227.1	206.7	218.3	141.7	93.6	34.7	8.9

and 1137± 21 mm during FO to WCI, and our estimation during May to January is just in between.

5.3. The uncertainties in energy budget of the "large lake"

The energy budget closure could reach 0.97 during the open water period of the "small lake" (Wang et al., 2017) while it could be 0.859 during July to November with the observations of radiation budget, turbulent heat flux and heat storage with a water depth of 35 m. The EBC value is quite high compared with the results of other energy budget studies (Nordbo et al., 2011; Mammarella et al., 2015). The turbulent heat flux, solar radiation and water temperature observations have quite different footprints and these mismatches will introduce uncertainty in these energy budget components. In addition, the distribution of solar radiation, the latent heat flux and sensible heat flux should be horizontally heterogeneous (Spence et al., 2011; Wang et al., 2014). Furthermore, the heat storage measured at a depth of 35 m in our study could only represent a good approximation. As shown in Fig. 9e and f, water temperature at a depth of 35 m has obvious diurnal variations (with maximum amplitude of approximately 6 °C in its diurnal variation) and seasonal variations (to a maximum value of approximately 10 °C), the heat transfer from water inflow, the heat stored in much deeper water, the heat transfer through horizontal advection and between water and sediment will all introduce uncertainty. In addition, sublimation during the winter period is none-zero over the "large lake", as a clear high *LE* during the ice-covered period could be observed by EC observation (Fig. 2f). Thus, the assumption of close to zero evaporation during the ice-covered period may not be the case.

6. Conclusions

Using eddy covariance observations in the Lake small Nam-Co ("small lake") and Lake Nam-Co ("large lake") on the TP, significant differences in lake-atmosphere boundary layer parameters, meteorological variables and turbulent heat fluxes are reported. Relative to the "small lake", the "large lake" has a larger depth and area; as a result, "large lake" has a larger thermal capacity, which could further lead to delayed dates of ice-formation and ice-melt, postponed peaks of seasonal variations of water surface temperature, air temperature, sensible heat flux and latent heat flux. In addition, the "large lake" has a lower water surface temperature, because it is more transparent to solar radiation and has a greater mixing layer depth and stronger turbulent mixing intensity in the water. The roughness length and bulk transfer coefficients for momentum are 80% and 7% higher, respectively, in the "large lake" than in the "small lake" because of its larger wind speed and higher wind-induced waves. The roughness lengths for heat and water of the "large lake" are approximately one order of magnitude lower than those in the "small lake", while the bulk transfer coefficients for heat and water at a height of 10 m and neutral condition show a 7% lower value in the "large lake". Thus, parameterization schemes for these coefficients should differ between small lakes and large lakes in numerical climate modeling. The total evaporation during the ice-free period of the "large lake" is estimated to be approximately 981 ± 18 mm during May to January, which is higher than the value of 812 mm during the open water period (from April to November) of the "small lake". Given quite close net radiation during open water periods of the two water bodies, the much higher evaporation in the "large lake" could be explained by the observed smaller *Bo* in the "large lake". Our conclusions could benefit scientific research on catchment-scale energy budgets and water balance analyses and lake modeling. The large discrepancy between our results and published model simulations suggest the need for a thorough evaluation of models' parameterization schemes when considering these high-elevation lakes.

Acknowledgements

This research has been funded by the Strategic Priority Research Program of Chinese Academy of Sciences(XDA20060101), the Chinese Academy of Sciences (QYZDJ-SSW-DQC019), the National Natural Science Foundation of China (41661144043, 41830650, 91637312, 41522501, 41705005 and 91737205), the China Postdoctoral Science Foundation, the "Hundred Talent Program" (Weiqiang Ma), and the ESA-MOST Dragon 4 project CLIMATE-TPE (Dragon 4 id. 32070). The MODIS data could be download freely from LAADS DAAC website (https://ladsweb.modaps.eosdis.nasa.gov/). The meteorological data of the Nam-Co station are accessible on the Third Pole Environment Database (http://en.tpedatabase.cn/portal/). The meteorological data in the "large lake" and eddy covariance observations used in this paper can be shared with the scientific public by emailing the corresponding author (wangbinbin@itpcas.ac.cn). We would like to thank the anonymous reviewers and the Editorial team of "Journal of Hydrology" for their good suggestions and comments.

Appendix A. Supplementary data

Supplementary data to this article can be found online at https://doi.org/10.1016/j.jhydrol.2019.03.066.

References

Andreas, E.L., Murphy, B., 1986. Bulk transfer coefficients for heat and momentum over leads and polynyas. J. Phys. Oceanogr. 16 (11), 1875–1883. https://doi.org/10.1175/1520-0485(1986) 016<1875:btcfha>2.0.co;2.

Beljaars, A., 1995. The impact of some aspects of the boundary layer scheme in the ECMWF model, Proc. Seminar on Parameterization of Sub-Grid Scale Physical Processes, Reading. ECMWF, United Kingdom.

Biermann, T., Babel, W., Ma, W., Chen, X., Thiem, E., Ma, Y., Foken, T., 2013. Turbulent flux observations and modelling over a shallow lake and a wet grassland in the Nam Co basin, Tibetan Plateau. Theor. Appl. Climatol 1–16. https://doi.org/10.1007/s00704-013-0953-6.

Blanken, P.D., Rouse, W.R., Schertzer, W.M., 2003. Enhancement of evaporation from a large northern lake by the entrainment of warm, dry air. J. Hydrometeorol. 4 (4), 680–693. https://doi.org/10.1175/1525-7541(2003) 004<0680:eoefal>2.0.co;2.

Brutsaert, W., 1982. Evaporation into the Atmosphere: Theory, History, and Applications. D. Reidel, Dordrecht, Netherlands.

Charnock, H., 1955. Wind stress on a water surface. Q. J. R. Meteorolog. Soc. 81 (350), 639–640. https://doi.org/10.1002/qj.49708135027.

Fairall, C.W., Bradley, E.F., Rogers, D.P., Edson, J.B., Young, G.S., 1996. Bulk parameterization of air-sea fluxes for tropical ocean-global atmosphere coupled-ocean atmosphere response experiment. J. Geophys. Res.: Oceans 101 (C2), 3747–3764. https://doi.org/10.1029/95JC03205.

Fang, X., Stefan, H.G., 1996. Dynamics of heat exchange between sediment and water in a lake. Water Resour. Res. 32 (6), 1719–1727. https://doi.org/10.1029/96WR00274.

Gao, Z., Wang, Q., Zhou, M., 2009. Wave-dependence of friction velocity, roughness lneght, and drag coefficient over coastal and open water surfaces by using three databases. Adv. Atmosph. Sci. 26 (5), 887–894.

Gerken, T., Babel, W., Herzog, M., Fuchs, K., Sun, F., Ma, Y., Foken, T., Graf, H.-F., 2015. High-resolution modelling of interactions between soil moisture and convective development in a mountain enclosed Tibetan Basin. Hydrol. Earth Syst. Sci. 4023–4040, pp. https://doi.org/10.5194/hess-19-4023-2015.

Gerken, T., Biermann, T., Babel, W., Herzog, M., Ma, Y., Foken, T., Graf, H.-F., 2014. A modelling investigation into lake-breeze development and convection triggering in the Nam Co Lake basin, Tibetan Plateau. Theor. Appl. Climatol. 117 (1–2), 149–167. https://doi.org/10.1007/s00704-013-0987-9.

Granger, R.J., Hedstrom, N., 2011. Modelling hourly rates of evaporation from small lakes. Hydrol. Earth Syst. Sci. 15 (1), 267–277. https://doi.org/10.5194/hess-15-267-2011.

Guo, Y., Zhang, Y., Ma, N., Song, H., Gao, H., 2016. Quantifying surface energy fluxes and evaporation over a significant expanding endorheic lake in the central tibetan plateau. J. Meteorol. Soc. Jpn 94 (5), 453–465. https://doi.org/10.2151/jmsj.2016-023.

Haginoya, S., Fujii, H., Kuwagata, T., Xu, J., Ishigooka, Y., Kang, S., Zhang, Y., 2009. Air-lake interaction features found in heat and water exchanges over nam co on the tibetan plateau. Sci. Online Lett. Atmosph. 5, 172–175. https://doi.org/10.2151/sola.2009-044.

Heiskanen, J.J., Mammarella, I., Ojala, A., Stepanenko, V., Erkkilä, K.-M., Miettinen, H., Sandström, H., Eugster, W., Leppäranta, M., Järvinen, H., Vesala, T., Nordbo, A., 2015. Effects of water clarity on lake stratification and lake-atmosphere heat exchange. J. Geophys. Res. Atmos. 120, 7412–7428. https://doi.org/10.1002/2014JD022938.

Immerzeel, W.W., van Beek, L.P.H., Bierkens, M.F.P., 2010. Climate change will affect the asian water towers. Science 328 (5984), 1382–1385. https://doi.org/10.1126/science.1183188.

Kropáček, J., Maussion, F., Chen, F., Hoerz, S., 2013. Analysis of ice phenology of lakes on the Tibetan Plateau from MODIS data. The Cryosphere. https://doi.org/10.5194/tc-7-287-2013.
Large, W.G., Pond, S., 1981. Open ocean momentum flux measurements in moderate to strong winds. J. Phys. Oceanogr. 11 (3), 324–336. https://doi.org/10.1175/1520-0485(1981) 011<0324:oomfmi>2.0.co;2.
Large, W.G., Pond, S., 1982. Sensible and latent heat flux measurements over the ocean. J. Phys. Oceanogr. 12 (5), 464–482. https://doi.org/10.1175/1520-0485(1982) 012<0464:salhfm>2.0.co;2.
Lazhu, K., Yang, J., Wang, Y., Lei, Y., Chen, L., Zhu, B. Ding, Qin, J., 2016. Quantifying evaporation and its decadal change for Lake Nam Co, central Tibetan Plateau. J. Geophys. Res.: Atmosph. 121 (13), 7578–7591. https://doi.org/10.1002/2015JD024523.
Li, W., Li, S., Pu, P., 2001. Estimates of Plateau lake evaporation: a case study of Zige Tangco. J. Lake Sci. (in Chinese) 13 (3), 227–232.
Li, X.-Y., et al., 2016. Evaporation and surface energy budget over the largest high-altitude saline lake on the Qinghai-Tibet Plateau. J. Geophys. Res.: Atmosph. 121 (18), 10470–410485. https://doi.org/10.1002/2016JD025027.
Li, X.-Y., Xu, H.-Y., Sun, Y.-L., Zhang, D.-S., Yang, Z.-P., 2007. Lake-Level change and water balance analysis at lake qinghai, west china during recent decades. Water Resour. Manage. 21 (9), 1505–1516. https://doi.org/10.1007/s11269-006-9096-1.
Li, Z., Lyu, S., Ao, Y., Wen, L., Zhao, L., Wang, S., 2015a. Long-term energy flux and radiation balance observations over Lake Ngoring, Tibetan Plateau. Atmosph. Res. 155, 13–25. https://doi.org/10.1016/j.atmosres.2014.11.019.
Li, Z., Lyu, S., Zhao, L., Wen, L., Ao, Y., Wang, S., 2015b. Turbulent transfer coefficient and roughness length in a high-altitude lake, Tibetan Plateau. Theor. Appl. Climatol. 1–13. https://doi.org/10.1007/s00704-015-1440-z.
Liu, H., Zhang, Q., Dowler, G., 2012. Environmental controls on the surface energy budget over a large southern inland water in the United States: an analysis of one-year Eddy Covariance flux data. J. Hydrometeorol. 13 (6), 1893–1910. https://doi.org/10.1175/JHM-D-12-020.1.
Liu, H.Z., Feng, J.W., Sun, J.H., Wang, L., Xu, A.L., 2014. Eddy covariance measurements of water vapor and CO2 fluxes above the Erhai lake. Sci. China: Earth Sci. (in Chinese) 44, 2527–2539. https://doi.org/10.1007/s11430-014-4828-1.
Liu, J., Wang, S., Yu, S., Yang, D., Zhang, L., 2009. Climate warming and growth of high-elevation inland lakes on the Tibetan Plateau. Global Planet. Change 67 (3), 209–217. https://doi.org/10.1016/j.gloplacha.2009.03.010.
Liu, W.T., Katsaros, K.B., Businger, J.A., 1979. bulk parameterization of air-sea exchange of heat and water vapor including the molecular constraints at the interface. J. Atmos. Sci. 36, 1722–1735. https://doi.org/10.1175/1520-0469(1979) 036<1722:BPOASE>2.0.CO;2.
Long, Z., Perrie, W., Gyakum, J., Caya, D., Laprise, R., 2007. Northern lake impacts on local seasonal climate. J. Hydrometeorol. 8 (4), 881–896. https://doi.org/10.1175/JHM591.1.
Lv, Y., 2008. Summertime numerical simulation and obervation of characteristic of ABL and local circulation over the Nam Co lake of the Tibetan Plateau. Phd. Thesis. Chinese Acadely of Sciences.
Ma, N., Szilagyi, J., Niu, G.-Y., Zhang, Y., Zhang, T., Wang, B., Wu, Y., 2016. Evaporation variability of Nam Co Lake in the Tibetan Plateau and its role in recent rapid lake expansion. J. Hydrol. 537, 27–35. https://doi.org/10.1016/j.jhydrol.2016.03.030.
Mammarella, I., Nordbo, A., Rannik, Ü., Haapanala, S., Levula, J., Laakso, H., Ojala, A., Peltola, O., Heiskanen, J., Pumpanen, J., et al., 2015. Carbon dioxide and energy fluxes over a small boreal lake in Southern Finland. J. Geophys. Res. Biogeosci. 120, 1296–1314. https://doi.org/10.1002/2014JG002873.
Ma, R., et al., 2011. China's lakes at present: number, area and spatial distribution. Sci. China Earth Sci. 54 (2), 283–289. https://doi.org/10.1007/s11430-010-4052-6.
Ma, Y., Zhu, Z., Zhong, L., Wang, B., Han, C., Wang, Z., et al., 2014. Combining MODIS, AVHRR and in situ data for evapotranspiration estimation over heterogeneous landscape of the Tibetan Plateau. Atmosph. Chem. Phys. 14, 1507–1515.
Mauder, M., Thomas, F., 2015. Eddy-Covariance Software TK3. zenodo. https://doi.org/10.5281/zenodo.20349.
Morrill, C., 2004. The influence of Asian summer monsoon variability on the water balance of a Tibetan lake. J. Paleolimnol. 32 (3), 273–286. https://doi.org/10.1023/B:JOPL.0000042918.18798.cb.
Nordbo, A., Launiainen, S., Mammarella, I., Leppäranta, M., Huotari, J., Ojala, A., Vesala, T., 2011. Long-term energy flux measurements and energy balance over a small boreal lake using eddy covariance technique. J. Geophys. Res.: Atmosph. 116 (D2), D02119. https://doi.org/10.1029/2010jd014542.
Oku, Y., Ishikawa, H., Haginoya, S., Ma, Y., 2006. Recent trends in land surface temperature on the Tibetan Plateau. J. Clim. 19 (12), 2995–3003. https://doi.org/10.1175/JCLI3811.1.
Panin, G.N., Nasonov, A.E., Foken, T., Lohse, H., 2006. On the parametersisaton of evaporation and sensible heat exchange for shallow lakes. Theor. Appl. Climatol. 85 (3–4), 123–129. https://doi.org/10.1007/s00704-005-0185-5.
Rouse, W.R., Oswald, C.J., Binyamin, J., Spence, C., Schertzer, W.M., Blanken, P.D., Bussières, N., Duguay, C.R., 2005. The role of northern lakes in a regional energy balance. J. Hydrometeorol. 6 (3), 291–305. https://doi.org/10.1175/JHM421.1.
Shi, X., Li, S., Andi, D. Li, Su, Z., 2010. A study of the change of Qinghai Lake evaporation. Climat. Environ. Res. (in Chinese) 15 (6), 787–796.
Singh, P., Nakamura, K., 2009. Diurnal variation in summer precipitation over the central Tibetan Plateau. J. Geophys. Res.: Atmosph. 114 (D20), D20107. https://doi.org/10.1029/2009jd011788.
Small, E.E., Kurc, S., 2001. The Influence of Soil Moisture on the Surface Energy Balance in Semiarid Environments, edited. Water Resources Research Institute, New Mexico.
Smith, S.D., 1988. Coefficients for sea surface wind stress, heat flux, and wind profiles as a function of wind speed and temperature. J. Geophys. Res. Oceans 93 (C12), 15467–15472. https://doi.org/10.1029/JC093iC12p15467.
Smith, S.D., 1989. Water vapor flux at the sea surface. Boundary-Layer Meteorol. 47 (1), 277–293. https://doi.org/10.1007/bf00122334.
Spence, C., Blanken, P.D., Hedstrom, N., Fortin, V., Wilson, H., 2011. Evaporation from Lake superior: 2: spatial distribution and variability. J. Great Lakes Res. 37 (4), 717–724. https://doi.org/10.1016/j.jglr.2011.08.013.
Tanny, J., Cohen, S., Assouline, S., Lange, F., Grava, A., Berger, D., Teltch, B., Parlange, M.B., 2008. Evaporation from a small water reservoir: Direct measurements and estimates. J. Hydrol. 351 (1–2), 218–229. https://doi.org/10.1016/j.jhydrol.2007.12.012.
Venalainen, A., Frech, M., Heikinheimo, M., 1999. Comparison of latent and sensible heat fluxes over boreal lakes with concurrent fluxes over a forest: implications for regional averaging. Agric. For. Meteorol. 98–99, 535–546.
Vickers, D., Mahrt, L., 2010. Sea-surface roughness lengths in the midlatitude coastal zone. Q. J. R. Meteorol. Soc. https://doi.org/10.1002/qj.617.
Verburg, P., Antenucci, J.P., 2010. Persistent unstable atmospheric boundary layer enhances sensible and latent heat loss in a tropical great lake: Lake Tanganyika. J. Geophys. Res. 115 (D11109). https://doi.org/10.1029/2009JD012839.
Wang, B., Ma, Y., Chen, X., Ma, W., Su, Z., Menenti, M., 2015. Observation and simulation of lake-air heat and water transfer processes in a high-altitude shallow lake on the Tibetan Plateau. J. Geophys. Res.: Atmosph. 120 (24), 12327–12344. https://doi.org/10.1002/2015JD023863.
Wang, B., Ma, Y., Ma, W., Su, Z., 2017. Physical controls on half-hourly, daily, and monthly turbulent flux and energy budget over a high-altitude small lake on the Tibetan Plateau. J. Geophys. Res.: Atmosph. 122 (4), 2289–2303. https://doi.org/10.1002/2016JD026109.
Wang, J., Zhu, L., Daut, G., Ju, J., Lin, X., Wang, Y., Zhen, X., 2009. Investigation of bathymetry and water quality of Lake Nam Co, the largest lake on the central Tibetan Plateau, China. Limnology 10 (2), 149–158. https://doi.org/10.1007/s10201-009-0266-8.
Wang, W., Wei, X., Cao, Ch., Gao, Z., Hu, Zh., Liu, Sh., Shen, Sh., Wang, L., Xiao, Q., Xu, J., Yang, D., Lee, X., 2014. Temporal and spatial variations in radiation and energy balance across a large freshwater lake in China. J. Hydrol. 511, 811–824. https://doi.org/10.1016/j.jhydrol.2014.02.012.
Webster, P.J., Lukas, R., 1992. TOGA COARE: The Coupled Ocean—Atmosphere Response Experiment. Bull. Am. Meteorol. Soc. 73 (9), 1377–1416. https://doi.org/10.1175/1520-0477(1992) 073<1377:tctcor>2.0.co;2.
Wei, D., Ri, X., Wang, Y., Wang, Y., Liu, Y., Yao, T., 2012. Responses of CO2, CH4 and N2O fluxes to livestock exclosure in an alpine steppe on the Tibetan Plateau, China. Plant Soil 359 (1–2), 45–55. https://doi.org/10.1007/s11104-011-1105-3.
Wen, L., Lyu, S., Kirillin, G., Li, Z., Zhao, L., 2016. Air-lake boundary layer and performance of a simple lake parameterization scheme over the Tibetan highlands. Tellus 2016. https://doi.org/10.3402/tellusa.v68.31091.
Wu, J., 1980. Wind-Stress coefficients over Sea surface near Neutral Conditions—A Revisit. J. Phys. Oceanogr. 10 (5), 727–740. https://doi.org/10.1175/1520-0485(1980) 010<0727:wscoss>2.0.co;2.
Wu, Y., Zheng, H., Zhang, B., Chen, D., Lei, L., 2014. Long-term changes of lake level and water budget in the Nam Co Lake Basin, Central Tibetan Plateau. J. Hydrometeorol. 15 (3), 1312–1322. https://doi.org/10.1175/jhm-d-13-093.1.
Xu, J., Yu, S., Liu, J., Haginoya, S., Ishigooka, Y., Kuwagata, T., Hara, M., Yasunari, T., 2009. The implication of heat and water balance changes in a lake basin on the tibetan plateau. Hydrol. Res. Lett. 3, 1–5.
Yang, K., Wu, H., Qin, J., Lin, C., Tang, W., Chen, Y., 2014. Recent climate changes over the Tibetan Plateau and their impacts on energy and water cycle: a review. Global Planet. Change 112, 79–91. https://doi.org/10.1016/j.gloplacha.2013.12.001.
Yu, S., Liu, J., Xu, J., Wang, H., 2011. Evaporation and energy balance estimates over a large inland lake in the Tibet-Himalaya. Environ. Earth Sci. 64 (4), 1169–1176.
Zeng, X., Zhao, M., Dickinson, R.E., 1998. Intercomparison of bulk aerodynamic algorithms for the computation of sea surface fluxes using TOGA COARE and TAO Data. J. Clim. 11 (10), 2628–2644. https://doi.org/10.1175/1520-0442(1998) 011<2628:IOBAAF>2.0.CO;2.
Zhang, B., Wu, Y., Zhu, L., Wang, J., Li, J., Chen, D., 2011. Estimation and trend detection of water storage at Nam Co Lake, central Tibetan Plateau. J. Hydrol. 405 (1), 161–170. https://doi.org/10.1016/j.jhydrol.2011.05.018.
Zhang, G., Yao, T., Xie, H., Zhang, K., Zhu, F., 2014. Lakes' state and abundance across the Tibetan Plateau. Chin. Sci. Bull. 59 (24), 3010–3021. https://doi.org/10.1007/s11434-014-0258-x.
Zhang, Qianyu, Liu, Heping, 2014. Seasonal changes in physical processes controlling evaporation over inland water: seasonal changes in lake evaporation. J. Geophys. Res. Atmos. 119 (16), 9779–9792. https://doi.org/10.1002/2014JD021797.
Zhou, S., Kang, S., Chen, F., Joswiak, D.R., 2013. Water balance observations reveal significant subsurface water seepage from Lake Nam Co, south-central Tibetan Plateau. J. Hydrol. 491, 89–99. https://doi.org/10.1016/j.jhydrol.2013.03.030.
Zhu, L., Xie, M., Wu, Y., 2010. Quantitative analysis of lake area variations and the influence factors from 1971 to 2004 in the Nam Co basin of the Tibetan Plateau. Chin. Sci. Bull. 55 (13), 1294–1303. https://doi.org/10.1007/s11434-010-0015-8.
Zilitinkevich, S., Mammarella, I., Baklanov, A., Joffre, S., 2008. The effect of stratification on the aerodynamic roughness length and displacement height. Boundary Layer Meteorol. 129 (2), 179–190. https://doi.org/10.1007/s10546-008-9307-9.